Marine Chemistry 241 (2022) 104104

Contents lists available at ScienceDirect

Marine Chemistry

journal homepage: www.elsevier.com/locate/marchem

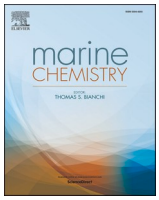

Bacterial sources and cycling dynamics of amino acids in high and low molecular weight dissolved organic nitrogen in the ocean

Hope L. Ianiri [a,*], Yuan Shen [a,b], Taylor A.B. Broek [a,c], Matthew D. McCarthy [a]

[a] Ocean Sciences Department, University of California, Santa Cruz, CA, USA
[b] State Key Laboratory of Marine Environmental Science & College of Ocean and Earth Sciences, Xiamen University, Xiamen, Fujian, China
[c] Lawrence Livermore National Laboratory, Livermore, CA, USA

ARTICLE INFO

Keywords:
Dissolved organic nitrogen
Amino acids
Molecular weight
Microbial degradation

ABSTRACT

Amino acids (AA) represent the most abundant identifiable biomolecule class in marine dissolved organic nitrogen (DON) and provide powerful proxies for DON degradation state. In particular, the D-enantiomers of AA (D-AA) are known to be derived mainly from bacteria, making them ideal tracers for bacterially derived N. However, despite the widespread use of D-AA tracers, it remains unclear if the accumulation of different D-AA species in the ocean indicates that most DON arises from direct bacterial sources or from continual bacterial alteration of eukaryotic algal material. This difference has major implications for our understanding of sources and cycling mechanisms of DON in the ocean. Here, we present the most extensive D-AA suite ever reported in younger, high molecular weight (HMW) DON contrasted with older, low molecular weight (LMW) solid phase extracted (SPE) DON from the central Atlantic and Pacific Oceans. We evaluate D-AA in these two contrasted MW fractions in the context of multiple common AA-based proxies and bulk DOM radiocarbon ($\Delta^{14}C$) data. Specifically, we assess if D-AA in HMW and LMW SPE-DON are most consistent with 1) preformed bacterial source signals, 2) progressive bacterial degradation/alteration of eukaryotic algal sources, or 3) gradual, continued resynthesis/addition of new bacterial biomolecules during ocean circulation. Our results suggest that AA-containing molecules in HMW and LMW SPE-DON fractions are almost entirely distinct, with independent bacterial sources and degradation mechanisms. In HMW DON, all measured indices support a surface-produced, semi-labile component which is progressively altered in the mesopelagic with increasing radiocarbon age. In contrast, for LMW SPE-DON, AA-based proxies showed conflicting results. Some proxies (D/L ratios of most D-AA, non-protein AA, mol% Gly, and %C-AA) indicated LMW SPE-DON was less labile and more degraded than HMW DON. However other proxies (D/L-Ala, the N isotope based ΣV parameter, and the commonly used DI index) indicated equivalent or even less degradation and resynthesis in the isolated LMW material compared to HMW material, suggesting a disconnect in the underlying mechanisms reflected by different proxies. Finally, AA composition and degradation state in the subsurface samples of both HMW and LMW DON varied little with increasing radiocarbon age, suggesting that HMW and LMW pools may cycle independently. Together, our results suggest that AA DON sources, while almost entirely bacterial, may be more diverse than previously believed, and that much of the hydrolysable AA pool in the ocean may not be derived from proteinaceous material. Overall, these observations support the microbial nitrogen pump idea, but with compositionally unique refractory components in both HMW and LMW material which resist degradation over millennial timescales.

1. Introduction

Marine dissolved organic matter (DOM) represents the largest pool of reduced carbon and nitrogen in the oceans, yet its long-term persistence remains an enigma. DOM is widely assumed to exist along a size-age-reactivity continuum, with high molecular weight (HMW) molecules representing young, semi-labile DOM while low molecular weight (LMW) molecules make up most of the old, refractory DOM (RDOM) (Walker et al., 2014, Walker et al., 2016, reviewed by Benner and Amon, 2015). Increasing evidence suggests that bacteria are a key player in forming RDOM, which persists for thousands of years (Gruber et al., 2006; Ogawa et al., 2001; Yamashita and Tanoue, 2008). This concept,

* Corresponding author at: University of California Santa Cruz, Ocean Sciences Department, Santa Cruz, CA 95064, USA.
E-mail address: hianiri@ucsc.edu (H.L. Ianiri).

https://doi.org/10.1016/j.marchem.2022.104104
Received 24 June 2021; Received in revised form 21 February 2022; Accepted 3 March 2022
Available online 9 March 2022

termed the microbial carbon pump (MCP, Jiao et al., 2010, 2011), has been studied at length (see reviewed literature in *The Microbial Carbon Pump in the Ocean*, edited by Jiao et al., 2011) and is supported by culturing studies (Gruber et al., 2006; Kawasaki and Benner, 2006; Lechtenfeld et al., 2015; Ogawa et al., 2001), in situ observations (Azam et al., 1983; Jørgensen et al., 2003; Nagata et al., 2003), and the extreme structural complexity dissolved organic carbon (DOC) fractions measured by high resolution mass spectrometry (Dittmar, 2015; Lechtenfeld et al., 2014). These observations, in context of a size-age-reactivity continuum, suggest that LMW RDOC is formed by progressive microbial degradation of semi-labile, HMW material.

However, investigation of bacterial production in dissolved organic nitrogen (DON), especially refractory DON (RDON), is far more limited. In large part this is due to the lack of methods available to isolate the entire DON pool, such that molecular study of RDON formation and cycling requires N-specific molecular level tracers, and typically isolation protocols. Most previous DON structural work focused only on HMW DON due to its ease of isolation by ultrafiltration methods (Aluwihare et al., 2005; Benner et al., 1997; McCarthy et al., 1998, 2007). However, in contrast to the complexity which characterizes DOC, early ^{15}N NMR studies indicated that most HMW DON is structurally simple, appearing almost entirely in amide form (Aluwihare et al., 2005; McCarthy et al., 1997), and likely composed mostly of proteinaceous material at subsurface depths (Aluwihare et al., 2005). While this presents a paradox in terms of the high lability of AA, these observations also underscore that AA-based proxies are the most powerful molecular-level biomarkers to investigate the DON pool. While standard hydrolytic molecular-level analysis only recovers a small portion of the AA which solid-state NMR suggests are present (generally ~10% of total DON; Benner, 2002; Kaiser and Benner, 2009), they nevertheless represent by far the largest identifiable biomolecules in DON. Importantly, they also represent by far the largest known *labile* N biochemical class. Thus, if bacteria form LMW RDON from semi-labile, HMW DON via a microbial nitrogen pump (Yamaguchi and McCarthy, 2018), analogous to the broader paradigm for the DOC pool, then a comparison of HMW versus LMW AA signatures should most clearly reflect progressive microbial alteration.

Almost all protein AA (except for Glycine) are chiral, meaning they have a L and D-enantiomer that have the same molecular formula, but are non-superimposable mirror images of each other. While all living organisms produce L-AA, prokaryotes represent the only major known source for D-AA (Radkov and Moe, 2014), meaning that D-AA are arguably the most direct bacterial biomarkers in marine DON (Broek et al., 2019; Kaiser and Benner, 2008; McCarthy et al., 1998). The abundance of D-AA directly correlates with both bacterial growth and degradation of organic matter (Kawasaki and Benner, 2006; Tremblay and Benner, 2009) and has been widely used to estimate contributions of bacterial OC and ON in sediments, particles and the DOM pool (Bourgoin and Tremblay, 2010; Kaiser and Benner, 2008; Kawasaki et al., 2011; Lehmann et al., 2020; Tremblay and Benner, 2006). Select D-AA are also highly abundant in marine DON, representing one of the central pieces of evidence for microbial origin (Broek et al., 2019; Kaiser and Benner, 2008; McCarthy et al., 1998).

However, despite the widespread use of D-AA as indicators of bacterial source and "degradation," a mechanistic understanding of D-AA patterns in terms of specific sources and cycling of marine DON is lacking. For example, marine DON D/L ratios do not increase with depth or age in HMW material, as would be expected if continued bacterial alteration resulted in a higher relative abundance of D-AA (Broek et al., 2019; McCarthy et al., 1998; Pèrez et al., 2003). In addition, D-Alanine (Ala), by far the most abundant D-AA species in DON, often exhibits depth trends opposite from other D-AA (Broek et al., 2019; Kaiser and Benner, 2008) and has been suggested to be as labile as its L-AA counterpart (Broek et al., 2019; Wang et al., 2020). Finally, multiple newly confirmed D-AA in the DON pool appear to behave differently in HMW versus LMW material (Broek et al., 2019). Such aspects suggest that a mechanistic understanding of bacterial processes responsible for marine RDON formation requires a clearer distinction between signatures of bacterial source versus often vaguely defined "degradation."

Evaluating multiple proxies for bacterial alteration and organic matter reactivity together represents one way to advance this mechanistic understanding. "Degradation" is a broad concept which can encompass multiple specific processes including bacterial biomass addition, eukaryotic biomolecule alteration, and selective removal. A range of AA-based proxies have been developed to measure overall degradation, typically based on observed differences in the AA composition of natural organic matter over range of reactivity (Cowie and Hedges, 1994; Dauwe et al., 1999; Dauwe and Middelburg, 1998), or in incubation studies (Amon et al., 2001; Calleja et al., 2013; Davis et al., 2009). Proxies commonly used include the relative abundance of nonprotein amino acids (NPAA) β-alanine (β-Ala) and γ-aminobutyric acid (γ-Aba) (Cowie and Hedges, 1994; Davis et al., 2009; Lee and Cronin, 1982) and protein AA glycine (Gly) (Dauwe and Middelburg, 1998; Kaiser and Benner, 2009; Lehmann et al., 2020; Nguyen and Harvey, 1997), the widely applied degradation index (DI) based on changes in mol % of multiple AA (Dauwe et al., 1999), and the carbon-normalized yield of AA (%C-AA) (Amon et al., 2001; Benner, 2002; Cowie and Hedges, 1994). In addition, the ΣV parameter is a relatively new index based on individual AA δ^{15}N isotope values. Autotrophic production with known δ^{15}N-AA patterns has ΣV values approximately between 0 and 1, and subsequent heterotrophic bacterial resynthesis adds bacterial biosynthate and alters the δ^{15}N-AA values, resulting in elevated ΣV values that are indicative of enhanced resynthesis (Calleja et al., 2013; McCarthy et al., 2007; Yamaguchi and McCarthy, 2018). Collectively, these AA-based proxies provide a range of potentially independent measures of bacterial source, reactivity, or degradation state of organic matter. However, past work has rarely explicitly considered how the different proxies coupled together may be interpreted mechanistically.

The overarching goal of this paper is to, for the first time, take a holistic approach which combines the diverse information of all these AA-proxies together with a recently expanded suite of D-AA tracers (Broek et al., 2019) to study the oceanic DON pool. We propose that together these data have the potential to unravel bacterial roles in DON preservation at a new mechanistic level. We report all these proxies for DON together, and then evaluate them in the context of both DOM molecular weight and Δ^{14}C from the surface to deep ocean in the central Atlantic and Pacific basins. This unique sample set allowed us to examine pathways of "pre-formed" bacterial surface source versus progressive bacterial degradation with DOM aging in some of the oldest and youngest components of the marine DON pool. We hypothesized that DON in the older waters in the deep Pacific would show evidence of more extensive degradation at the molecular level compared to the younger deep waters in the Atlantic, consistent with previous reports of lower concentrations of DOC and biochemicals in unfiltered deep water in the central Pacific compared to central Atlantic (Hansell and Carlson, 1998; Kaiser and Benner, 2009). Additionally, if it is assumed that DON follows a size-age-reactivity continuum similar to DOC (Amon and Benner, 1994, 1996; Walker et al., 2014, 2016), we would expect DON molecular composition to reflect progressive bacterial degradation of HMW DON to form more stable, refractory LMW DON. Using our comprehensive dataset including AA proxies and Δ^{14}C ages of isolated DON size fractions, we directly test both hypotheses.

2. Methods

2.1. DOM sample collection and molecular weight isolation

DOM samples were collected in the North Atlantic Subtropical Gyre at BATS (31°40′N, 64°10′W) aboard the *R/V Atlantic Explorer* in August 2015 and May 2016 and in the North Pacific Subtropical Gyre at HOT Station ALOHA (22°45′N, 158°00′W) aboard the *R/V Kilo Moana* in

August 2014 and May 2015 as described in Broek et al. (2017). Surface seawater samples were collected via underway sampling systems at approximately 7.5 m on the *R/V Kilo Moana* and 2 m on the *R/V Atlantic Explorer*. Large volume subsurface samples (~1000 L to 4300 L) were collected via Niskin bottles at depths of 400 m, 850 m, and 2500 m. Full details of the sampling and sample isolation protocols are described in Broek et al. (2017). Briefly, all seawater was filtered through 53 μmol Nitex mesh and pumped through 0.2 μmol cartridge filters. Subsamples for total DOM were frozen in pre-combusted glass vials. HMW DOM was concentrated using large volume tangential-flow ultrafiltration (UF) using four spiral wound PES UF membranes with a molecular weight cut off of 2.5 kDa (GE Osmonics) and a concentration factor of approximately 1000. The LMW SPE-DOM was collected via solid-phase extraction of the UF permeate using PPL sorbent (Agilent Bondesil PPL), as described previously (Broek et al., 2017). After desalting via diafiltration (for HMW) and rinsing the resin with DI water (for LMW), both fractions were lyophilized and stored as dry powder until analysis.

A sample representing the entire UF permeate would have been thousands of liters of seawater, so to avoid or minimize contamination during the long-duration sampling and filtration, the UF permeate was subsampled at constant time intervals throughout the ultrafiltration (after protocols first described in Benner et al., 1997). This composite permeate sample was used to evaluate expected concentrations in each experiment. Notably, however, because permeate becomes progressively more concentrated throughout ultrafiltration (e.g., Walker et al., 2011), exact mass balance was not possible based on this sampling protocol, which was intended only as a general check on expected recoveries (Broek et al., 2017). Because a rigorous mass balance approach to permeate sampling was not part of the experimental protocol, any individual permeate concentration measurements must be interpreted with caution.

2.2. Bulk elemental analyses

DOC, DON, %OC, and %ON data were published previously (Broek et al., 2017). Briefly, DOC and TDN concentrations in total DOM and the UF permeate were measured using high temperature oxidation with a Shimadzu TOC-V as contract samples in the Carlson lab at the University of California, Santa Barbara. Total dissolved inorganic N (DIN) concentrations were determined using a Lachat QuickChem 8000 Flow Injection Analyzer. Total DON concentrations were determined by subtracting DIN from TDN. This measurement was not made in the UF permeate due to the mass balance considerations discussed in Section 2.1 combined with the subtraction of much greater DIN concentrations from low natural abundance DON. Weight %OC and %ON of DOM size fractions were determined via elemental analyzer isotope ratio mass spectrometry (EA-IRMS) using a Carlo Erba CHNS-O EA1108-elemental analyzer interfaced via a ConFlo III device with a ThermoFinnigan Delta Plus XP isotope ratio mass spectrometer at the University of California Santa Cruz (UCSC) Stable Isotope Laboratory (SIL).

2.3. GC–MS and GC-IRMS sample preparation

To isolate AA for gas chromatograph mass spectrometry (GC–MS) and GC- isotope ratio mass spectrometry (IRMS) analysis, HMW DON and LMW SPE-DON samples were first hydrolyzed using liquid-state (6 N HCl) acid hydrolysis according to standard conditions (Calleja et al., 2013; Kaiser and Benner, 2005; Silfer et al., 1991). Following the hydrolysis, a norleucine (Nle) internal standard was added to each sample, and hydrolysates were dried under N_2 gas at 60 °C. The dry samples were then redissolved in 0.1 N HCl, filtered with a 0.7 μm GFF filter, and purified using cation-exchange chromatography with Bio-Rad AG50W-X8 resin (200–400 mesh) and eluted with ammonium hydroxide according to Takano et al. (2010). Ammonium hydroxide was removed with N_2 gas, and samples were reprotonated with 0.2 N HCl at 110 °C for 5 min. Trifluoroacetyl isopropyl ester (TFAiP) derivatives were prepared according to Décima et al. (2017) and Silfer et al. (1991). Finally, AA were purified using liquid-liquid extraction after Ueda et al. (1989). Samples were stored at −20 °C until analysis, at which point they were dried under N_2 gas and dissolved in ethyl acetate for analysis.

2.4. GC–MS analysis and quantification of AA

AA D/L ratios of HMW and LMW SPE-DON at BATS (2015, 2016) were measured using GC–MS analysis and AA structural identities were verified based on MS fragmentation according to established protocols from the McCarthy lab (Broek et al., 2019; Yamaguchi and McCarthy, 2018). An Agilent 7890A/5975B gas chromatograph mass spectrometer equipped with an Altech Chirasil-L-Val column (50 m × 0.25 mm, 0.16 μm thick) was used to analyze D and L-AA in HMW DON and LMW SPE-DON. 1 uL of sample was injected through a splitless inlet at 200 °C with a helium gas carrier flow rate of 0.9 mL/min. AA were separated using a 4-ramp temperature program: initial temperature of 45 °C; ramp 1: 2 °C/min to 75 °C; ramp 2: 4 °C/min to 110 °C; ramp 3: 1 °C/min to 125, ramp 4: 4 °C/min to 200 °C, 2.5 min hold. Single ion monitoring was used to identify each AA using the following characteristic major ion fragments (*m/z*): L and D-Ala, 140; L and D-Valine (Val), 168; L-Threonine (Thr), 153; Glycine (Gly), 126; L-Isoleucine (Ile), L and D-Leucine (Leu), L-Nle, 182; L and D-Serine (Ser), 138; L-Proline (Pro), 166; L and D- asparagine + aspartic acid (Asx), 184; L and D- glutamine + glutamic acid (Glx), 180; L and D-Lysine (Lys) 180; L and D-Phenylalanine (Phe), 190; L and D-Tyrosine (Tyr), 203. For AA with the same characteristic fragment ion (Glx and Lys), identification was made based on retention time using external standards. Acid hydrolysis cleaves the terminal amine of glutamine and asparagine, converting them to glutamic acid and aspartic acid, meaning combined concentrations are measured and reported as "Glx" and "Asx." A response factor was calculated for each AA from a linear four-point calibration curve to determine AA concentration. The average standard deviation of triplicate measurements was ±7.23% of total peak area for HMW DOM and ± 14.6% of the total peak area for LMW SPE-DOM samples, while the average internal standard recovery was similar for both size fractions (~60%).

2.5. GC-IRMS analysis of AA

To calculate the compound-specific $\delta^{15}N$-based degradation parameter ΣV, $\delta^{15}N$-AA measurements were also made on a subset of the samples measured for AA D/L ratios, including HMW and LMW SPE-DON collected at HOT in 2015 and BATS in 2016. All isotopic analyses were completed at the UCSC-SIL according to established protocols of the McCarthy Lab (McCarthy et al., 2013; Shen et al., 2021; Yamaguchi and McCarthy, 2018). Following hydrolysis and column chromatography as detailed above, AA were further purified via HPLC and collected as separate fractions according to Broek et al. (2013) and Broek and McCarthy (2014). The purified AA fractions were then recombined for further analysis. TFAiP derivatives were made and purified via liquid-liquid extraction as detailed above (Section 2.3). A Thermo Trace Ultra gas chromatograph coupled with a Finnigan MAT DeltaPlus XL IRMS at UCSC SIL was used for GC-IRMS analysis. AA were separated on a BPX-5 column (60 m × 0.32 mm, 1.0 μmol film thickness) for $\delta^{15}N$ analysis. Samples were injected in triplicates. A total of twelve AA were measured, including Ala, Gly, Thr, Ser, Val, Leu, Ile, Pro, Asx, Glx, Phe, and Lys. The $\delta^{15}N$ value of AA is reported relative to N_2 in air: $\delta^{15}N$ (‰) vs. air $= \{[(^{15}N/^{14}N)_{sample}/ (^{15}N/^{14}N)_{air}]\text{-}1\} \times 1000$.

2.6. HPLC sample preparation, analysis, and quantification of D and L-AA

Concentrations of D- and L-enantiomers of AA in total DOM, UF permeate, HWM DON, and LMW SPE-DON from HOT (2014, 2015) and BATS (2015, 2016) were determined using an Agilent 1260 ultrahigh performance liquid chromatography (UPLC) system equipped with a

fluorescence detector (excitation: 330 nm; emission: 450 nm) after Shen et al. (2017). HMW and LMW SPE-DON samples were hydrolyzed as detailed above using 6 N HCl at 110 °C for 20 h (Kaiser and Benner, 2005; Silfer et al., 1991). Total DOM and UF permeate samples were hydrolyzed using a vapor-phase technique with 6 N HCl at 150 °C for 32.5 min (Kaiser and Benner, 2005). Derivatization followed protocols of Kaiser and Benner (2005) using o-phthaldialdehyde and N-isobutyryl-L-cysteine (OPA/IBLC). Samples were then separated on a Poroshell 120 EC-C18 (4.6 × 100 mm, 2.7 μm particles) column with a linear binary gradient starting with 100% potassium di-hydrogen phosphate (KH_2PO_4; 48 mmol L^{-1}, pH = 6.25) to 61% KH_2PO_4 and 39% methanol: acetonitrile (13:1, *v*/v) at 13.3 min, 46% KH_2PO_4 at 19.2 min, 40% KH_2PO_4 at 21.3 min, and 20% KH_2PO_4 at 22 min. Concentrations of L and D-Asx, L and D-Glx, L and D-Ser, L-His, Gly, L-Thr, β-Ala, L-Arg, L and D-Ala, γ -Aba, L-Tyr, L-Val, L -Phe, L- Ile, L- Leu, and L-Lys were determined from external standards of known concentrations. The limit of quantification for individual AA is ~0.5 nmol/L.

2.7. Racemization correction

Hydrolysis conditions for GC–MS, GC-IRMS, and HPLC analyses were identical to those reported in Kaiser and Benner (2005), and racemization was corrected according to Kaiser and Benner (2005). For GC–MS and GC-IRMS analyses, racemization corrections for derivatization via TFAiP were determined independently for each amino acid by measuring the amount of D enantiomer produced in the "Pierce H" commercial L Amino Acid standard, containing equivalent molar amounts of all AA investigated in this study (Thermo Scientific, 2.5 μmol/mL), derivatized in the same batch as samples.

Derivatization with OPA/IBLC (used for HPLC analyses) does not induce racemization. However, blank corrections were made for background enantiomeric values of the reagents. No racemization was observed during the column chromatography or base dry down (Broek et al., 2019). Thus, for all samples the total racemization blank is the sum of the hydrolysis blank and the derivatization blank. For HPLC analyses utilizing vapor phase hydrolysis, the average total racemization blank was 4.7%D (relative to all total AA, or equivalent to a D/L ratio of 0.05), while for HPLC analyses utilizing liquid-phase hydrolysis, the average total racemization blank was 1.9% (D/L ratio of 0.02). For GC–MS analyses, the average total racemization blank was 2.0% D (D/L ratio 0.02).

2.8. Data synthesis and analysis

By combing HPLC and GC–MS analyses, we measured a total of nine D-AA, thirteen L-AA, one achiral protein AA (Gly), and two NPAA (β-Ala, and γ-Aba) (Supplementary 2.0). Because all samples investigated in this study (total DOM, HMW DOM, SPE-DON, and UF permeate) were analyzed via HPLC, for consistency, all analyses (besides isotopic measurements) are reported as measured HPLC-based concentrations whenever possible. The exceptions are the D-AA with concentrations too low to be measured via HPLC, and so only quantified by GC–MS (D-Val, D-Leu, D-Phe, D-Tyr, and D-Lys). Additionally, the D/L ratios of the D-AA only measured by GC–MS are reported as the ratio of D to L-AA concentration measured by GC–MS. Finally, to compare this expanded suite of D and L-AA between ocean basins, we also included previously published GC–MS data at HOT for D-AA which were measured only by GC–MS (D-Leu, D-Val, and D-Phe, Broek et al., 2019).

Analyses were completed in Microsoft Excel 365 and R (4.0.5) (R Core Team, 2021). Data were tested for normality using the Shapiro-Wilk test. Statistical differences between means were analyzed using the Welch's two-sample *t*-test for normally distributed data and the nonparametric Mann-Whitney *U* test for nonnormal data. To test for significant differences between the slope and y-intercept of linear regression lines, analysis of covariance (ANCOVA) was performed. A 95% confidence interval was used for all statistical tests. Principal component analysis (PCA) was performed using AA-based proxies (D-AA yield, L-AA yield, %C-AA, Mol % Gly, %NPAA, and DI) and D/L ratios (D/L-Ala, D/L-Asx, D/L-Glx, D/L-Ser, D/L-Leu, D/L- Val, and D/L-Phe) of HMW and LMW SPE-DON. Variables that were not measured in all DOM samples (D/L-Tyr, D/L-Lys, and ΣV) were excluded from the analysis. All variables were scaled to unit variance prior to analysis.

Degradation index (DI) values were calculated according to Dauwe et al. (1999) using the formula $DI = \Sigma[(AA_i - AVG\ AA_i)/SD\ AA_i \times \text{factor coefficient}_i]$, where AVG AA_i and SD AA_i are the average and standard deviation of mol % for each AA of sample *i*. Factor coefficients from Kaiser and Benner (2009) and Peter et al. (2012) specific for marine DOM were applied. The ΣV parameter was calculated according to McCarthy et al. (2007), using the equation $\Sigma V = 1/n \times \Sigma Abs(\chi_{AAi})$, where *n* is the total number of trophic AA included in the calculation (Glx, Asx, Ala, Ile, Leu, Pro, Val), and χ_{AAi} is the difference in $\delta^{15}N$ value between each individual trophic AA and the average of all trophic AA. Autotrophic biomass typically has a ΣV value between 0 and 1, thus any ΣV values greater than this indicates bacterial processes causing isotopic fraction of AA regardless of compound type or organic matter matrix. Total %D was calculated with and without D-Ala, as Total %D = Σ[D-AA] nmol/L / Σ([L-AA] + [D-AA]) nmol/L. Only AA measured in all samples (all L and D-AA except D-Tyr and D-Lys) were included in this calculation for direct comparison.

2.9. Terminology

"HMW DOM/N" and "LMW SPE-DOM/N" are used to refer to the individually isolated size fractions, as described in Section 2.1 and in Broek et al. (2017). We note that the samples analyzed here are subsamples of those same samples whose collection was reported in that paper. "HMW" refers to ultrafiltered DOM between 0.2 μm and 2.5 kDa, which in this sample set had $\Delta^{14}C$ values ranging from −37.3‰ ± 3.8‰ (surface) to −365.7‰ ± 2.3‰ (2500 m) (240 to 3595 yr BP) at HOT and − 43.0‰ ± 3.2‰ (surface) to −304.2‰ ± 1.9‰ (2500 m) (355 to 2915 yr BP) at BATS (Broek et al., 2017, 2020). "LMW SPE" refers to solid-phase extracted (PPL resin) DOM from the permeate of HMW DOM (smaller than 2.5 kDa), which had $\Delta^{14}C$ values ranging from −343.0‰ ± 2.3‰ (surface) to −577.6‰ ± 1.7‰ (2500 m) (3310 to 6860 yr BP) at HOT and − 316.1‰ ± 2.0‰ (surface) to −485.5‰ ± 1.9‰ (850 m) (3050 to 5340 yr BP) at BATS (Broek et al., 2017, 2020).

Most AA-based proxies utilized in this study have been used by past work to indicate generalized "degradation" or "degradation state." However, bacterial degradation includes many different, simultaneous processes. While these processes will together contribute to the overall "degradation state" of an organic sample, one goal of this paper is to try to understand the mechanistic underpinnings of independent proxies and interpret differences between them for DON. We thus define here how we use terms representing bacterial source and individual degradation processes/mechanisms in the text below (see also Table S1): **"Bacterial source"** refers to prokaryotic biosynthate, as opposed to eukaryotic biosynthate. We use **"heterotrophic resynthesis"** to refer to any changes that occur within a bacterial cell resulting in new synthesis of bacterial biomolecules, or prokaryote biosynthate. Thus, heterotrophic resynthesis results in a bacterial source, although this could include intact cells, altered fragments of bacterial cells, or simply bacterial biomolecules. In contrast, we use "**degradation**" as it is commonly used in the literature, to refer to the effect of a wider range of microbial processes, including alteration of molecular structure, selective removal of labile biomolecules, or addition of new bacterial biomass. Notably, bacterial degradation processes only result in a "bacterial source" when there is an input of bacterially produced molecules to the DON pool (such as addition of new bacterial biomass). In contrast, bacterial degradation can also selectively remove labile biomolecules from eukaryotic biosynthate, in which case remaining material might not have any molecules synthesized by bacteria themselves, meaning there is no bacterial "source" detected.

3. Results

3.1. L-AA and D-AA concentrations in total DOM

Total hydrolysable L-AA and D-AA concentrations were greater at HOT than BATS in the surface, while at 2500 m the concentrations were greater at BATS than HOT (Fig. 1, Table S2). At HOT, the maximal L-AA and D-AA concentrations were observed in the surface, averaging 209.7 ± 17.4 nmol/L for L-AA and 48.5 ± 2.3 nmol/L for D-AA between the two sampling years (2014 and 2015). L-AA and D-AA concentrations decreased substantially between the surface and 400 m, then continued to decrease slightly between 400 m and 2500 m. The lowest concentrations were observed at 2500 m, averaging 47.6 ± 6.8 nmol/L L-AA and 8.9 ± 0.8 nmol/L D-AA. Concentrations of both enantiomers were similar between the two sampling years.

At BATS, maximal D-AA concentrations were also observed at surface, with an average of 27.1 ± 3.3 nmol/L between sampling years (Fig. 1, Table S2). Contrary to the case at HOT, there were notable differences in measured AA concentrations between different sampling years throughout the water column (see Supplementary 1.0). The depth of maximal L-AA concentrations varied between sampling years; in 2016 (May) the highest L-AA concentrations were measured at the surface (138.5 nmol/L) while in 2015 (August) the highest L-AA concentrations were measured at 400 m (166.8 nmol/L). In 2015, minimum L-AA and D-AA concentrations were observed at 2500 m depth (53.9 nmol/L and 13.2 nmol/L, respectively), while in 2016, minimum L-AA and D-AA concentrations were observed at 850 m (66.4 nmol/L and 15.3 nmol/L, respectively).

3.2. Recovery of HMW and LMW SPE-DON fractions

Complete DOC and DON recovery data from total DOM for these same HMW and LMW SPE-DOM size fractions have been published and extensively discussed previously (Broek, 2019; Broek et al., 2017, 2020). Briefly, the average total DOC recovery across all depths, stations, and sampling seasons was significantly greater in the LMW SPE-DOM fraction (26.7% ± 6.7%) than the HMW DOM fraction (10.1% ± 3.2%) (Welch's two-sample *t*-test, $p < 0.001$) (Table 1). In contrast, the average total DON recovery at all depths, stations, and sampling seasons was not significantly different in HMW DOM versus LMW SPE-DOM, both averaging 13.3% ± 5.4% (Welch's two-sample *t*-test, $p = 0.138$).

The percent of hydrolysable AA from total DOM recovered in each size fraction was determined based HPLC measurements of AA in total DOM samples. The percent of total AA recovered in the HMW DOM size fraction was significantly greater than the LMW SPE-DOM size fraction across all depths, stations, and sampling seasons (Welch's two-sample *t*-test, $p < 0.001$) (Table 1). There was no significant difference in AA recovery from total DOM for HMW DON at HOT versus BATS, with an average AA recovery of 25.3% ± 0.8% at both sites. In contrast, AA recovery of LMW SPE-DON was significantly greater at BATS (15.6% ± 3.4%) than HOT (9.9% ± 3.2%) (Welch's two-sample *t*-test, $p = 0.0082$). The combined AA recovery of HMW and LMW DOM was not significantly different between HOT and BATS, averaging 37.9% ± 9.2% over all depths and sampling seasons.

The percent of DOC and hydrolysable AA from the UF permeate recovered in LMW SPE-DOM was also determined based on HPLC measurements of the UF permeate subsamples, with permeate composites representing an approximation of total LMW DOM (Table 1). Taking into account the caveats about permeate mass balance noted above (Section 2.1), the recovery of DOC in LMW SPE-DON from the UF permeate averaged across all depths was significantly greater at BATS than HOT, averaging 38.8% ± 6.3% and 25.4% ± 11.0%, respectively (Welch's two-sample *t*-test, $p = 0.0132$). In contrast, the recovery of AA in LME SPE-DON from the UF permeate averaged across all depths was not statistically different at HOT and BATS, averaging 17.8% ± 5.3% and 20.3% ± 5.8%, respectively (Welch's two sample *t*-test, $p = 0.7074$). These values were therefore somewhat greater than total DON recovery in the SPE-DON fraction noted above.

3.3. L and D-AA yield of HMW and LMW SPE-DON

Overall, AA concentrations as measured by HPLC and GC–MS were similar (Supplementary 2.0, Fig. S1). In the HMW size fraction, total D-AA yields (μmol D-AA normalized to mg total organic nitrogen, μmol/mgN) were significantly greater at HOT than BATS at all depths (Fig. 2, Table S3). Average HMW L-AA yields (μmol/mgN) from both cruises were also greater at HOT than BATS, though these differences were not universally greater than analytical error (Fig. 2). In HMW DON, the L-AA yield decreased from an average surface maximum of 6.1 ± 1.0 μmol/mgN at HOT and 5.6 ± 0.9 μmol/mgN at BATS to average deep (2500 m) values of 4.1 ± 0.4 μmol/mgN at HOT and 3.6 ± 0.5 μmol/mgN at BATS. The D-AA yield of HMW DON showed an opposite trend to the L-AA yield: D-AA yields increased from average surface values of 0.82 ± 0.01 μmol/mgN at HOT and 0.70 ± 0.08 μmol/mgN at BATS to average maximum values at 400 m of 0.90 ± 0.03 μmol/mgN at HOT and 0.71 ± 0.06 μmol/mgN at BATS. At both stations, from the maxima at 400 m, D-AA yields decreased to minimum at 2500 m depth, averaging 0.76 ± 0.02 μmol/mgN at HOT and 0.66 ± 0.06 μmol/mgN at BATS.

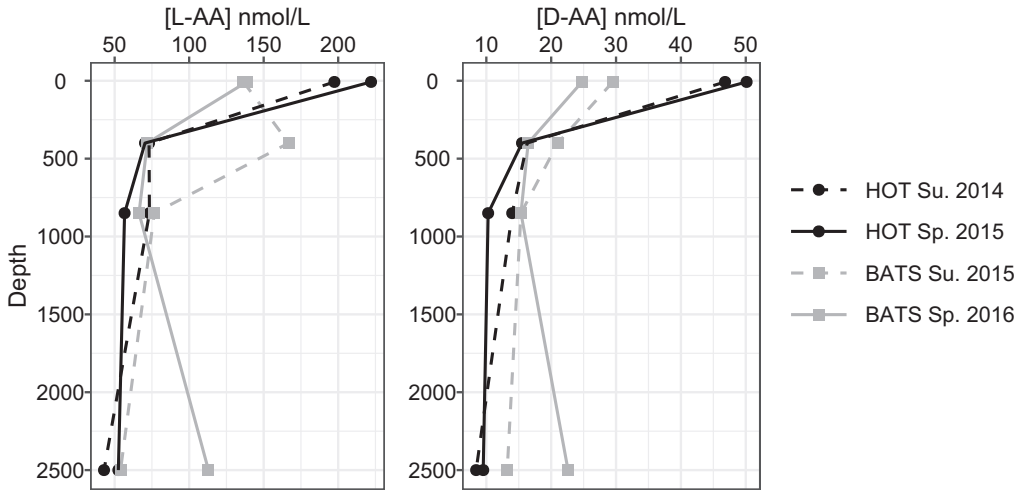

Fig. 1. Total dissolved hydrolysable L-AA and D-AA concentrations (nmol/L) at HOT (black circles) and BATS (grey squares) measured in summer ("Su.," dashed lines) and spring ("Sp.," solid lines) cruises.

Table 1
Total hydrolysable amino acids (AA), organic carbon (OC), and organic nitrogen (ON) recoveries of HMW UDOM and LMW SPE-DOM (PPL extract of ultrafiltration permeate). Recovery values are relative to hydrolysable AA, OC, and ON concentrations in 0.2 μm filtered seawater unless otherwise noted.

Location	Type	C/N	±	%AA	±	%DOC	±	%DON	±	n
HOT	HMW UDOM	12.44	0.6	27.42	8.61	10.58	4.15	13.61	4.09	8
BATS	HMW UDOM	12.27	0.6	22.9	7.14	9.74	1.94	11.08	3.69	7
HOT	LMW SPE-DOM	26.95	1.5	9.94	3.23	23.38	6.06	13.12	4.73	8
BATS	LMW SPE-DOM	24.78	0.2	15.63	3.69	31.16	5.36	16.29	7.46	7
HOT	LMW SPE-DOM from UF permeate	ND	ND	17.8	5.3	25.4	11.0	ND	ND	8
BATS	LMW SPE-DOM from UF permeate	ND	ND	20.3	5.8	38.8	6.3	ND	ND	7
HOT	Total extracted DOM	ND	ND	37.36	9.2	33.96	7.34	26.73	6.25	16
BATS	Total extracted DOM	ND	ND	38.53	8.03	40.9	5.7	27.37	8.32	14

In LMW SPE-DON, the L-AA and D-AA yields were lower than observed in HMW DON throughout the water column in both ocean basins (Fig. 2, Table S3). Unlike HMW DON, the L-AA and D-AA yields in LMW SPE-DON were very similar between ocean basis, with values within propagated error between the HOT and BATS sites at most depths. At all sites L-AA and D-AA yields were both greatest at the surface and decreased into the mesopelagic, but then were relatively constant with depth. L-AA yields at the surface averaged 2.7 ± 0.2 μmol/mgN at HOT and 2.4 ± 0.2 μmol/mgN at BATS and at 2500 m averaged 1.36 ± 0.06 μmol/mgN at HOT and 1.3 ± 0.1 μmol/mgN at BATS. LMW D-AA yields in the surface averaged 0.35 ± 0.03 μmol/mgN at HOT and 0.340 ± 0.003 μmol/mgN at BATS and at 2500 m averaged 0.200 ± 0.004 μmol/mgN at HOT and 0.170 ± 0.001 μmol/mgN at BATS. In contrast to HMW D-AA data, there was no maxima in the D-AA yield at 400 m.

3.4. AA composition of HMW and LMW SPE-DON: D/L ratios and molar abundance

Few significant differences in depth-averaged AA D/L ratios were observed between HOT and BATS within either size fraction (Fig. 3). In HMW DON, average D/L ratios of Leu and Phe were significantly greater at HOT compared to BATS (Welch's two-sample *t*-test, $p < 0.05$), however absolute offsets were very small (0.02–0.03), and close to the percent fractional uncertainty (30–50%). In LMW SPE-DON, no AA had significantly different D/L ratios between the two ocean basins. Similarly, depth profiles of D/L AA ratios were exceptionally consistent between BATS and HOT in both size fractions, with values within error for all AA at almost all depths (Fig. 4). In LMW SPE-DON, most AA had a maximum D/L ratio at 400 m, while depth trends in the HMW DON were more variable.

Within each ocean basin, however, the average D/L ratios of most AA were significantly different between the two molecular weight fractions (Fig. 3). However, the specifics differed with ocean basin and size fraction. At HOT and BATS, only D/L-Ala was significantly greater in HMW DON compared to LMW SPE-DON (Mann Whitney *U* test, $p < 0.001$), while D/L-Asx, D/L-Glx, D/L-Leu, D/L-Val, and D/L-Phe were significantly greater in LMW SPE-DON compared to HMW DON (Welch's two-sample *t*-test/Mann Whitney *U* test, $p < 0.001$). At HOT, D/L-Ser was also significantly greater in LMW SPE-DON than HMW DON (Welch's two-sample *t*-test, $p < 0.001$). At BATS, D-Tyr and D-Lys were measured above blank values in almost all LMW SPE-DON samples; however, they were indistinguishable from blank values in multiple HMW samples (Fig. 4, Table S4). D-Tyr and D-Lys were not measured in the previously published GC–MS analyses at HOT and cannot be observed by the HPLC method used here, thus are not reported in this ocean basin.

Within each size fraction, the average relative molar abundance of each AA was also similar between HOT and BATS, with mol% values for all AA at most depths within error at HOT and BATS (Fig. S2, Table S5). However, relative molar abundance of individual AA was markedly different in HMW vs. LMW SPE-DON. At BATS, the average molar abundance of Ala and Ser was significantly higher in HMW DON than LMW SPE-DON (Welch's two-sample *t*-test, $p < 0.05$), while Gly, Asx, Glx, Leu, Phe, and Tyr were higher in LMW SPE-DON than HMW DON (Welch's two-sample *t*-test, $p < 0.05$). At HOT, molar abundance of Ala, Ser, and Thr was significantly greater in HMW than LMW SPE-DON (Welch's two-sample *t*-test, $p < 0.05$), while Gly, Asx, Glx, Leu, Val, Phe, and Tyr were significantly greater in LMW SPE-DON than HMW DON (Welch's two-sample *t*-test/Mann Whitney *U* test, $p < 0.05$).

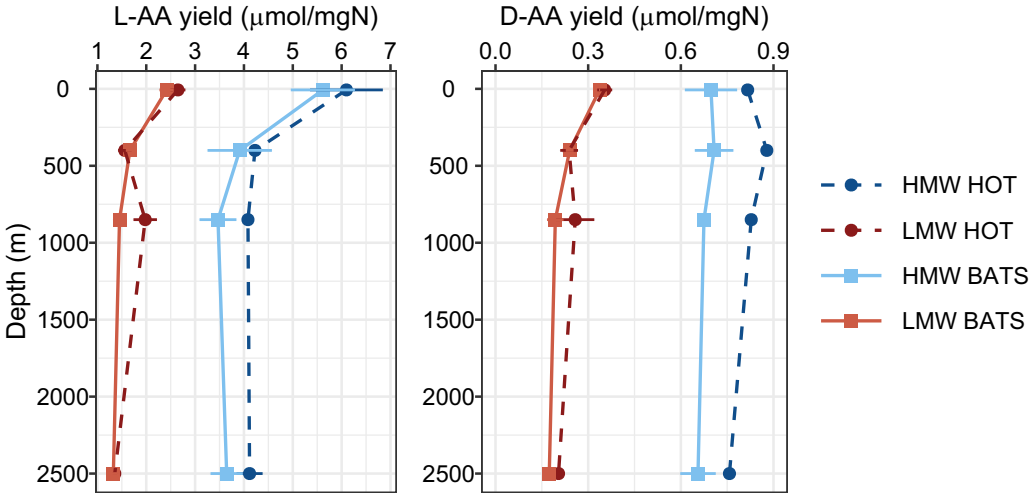

Fig. 2. L-AA and D-AA yields normalized to mg total organic nitrogen (μmol/mgN) in HMW DON (blue) and LMW SPE-DON (red) at HOT (circles, dashed line) and BATS (squares, solid line). Error bars represent the mean deviation of spring and summer cruise data and are smaller than symbol where not visible. (For interpretation of the references to colour in this figure legend, the reader is referred to the web version of this article.)

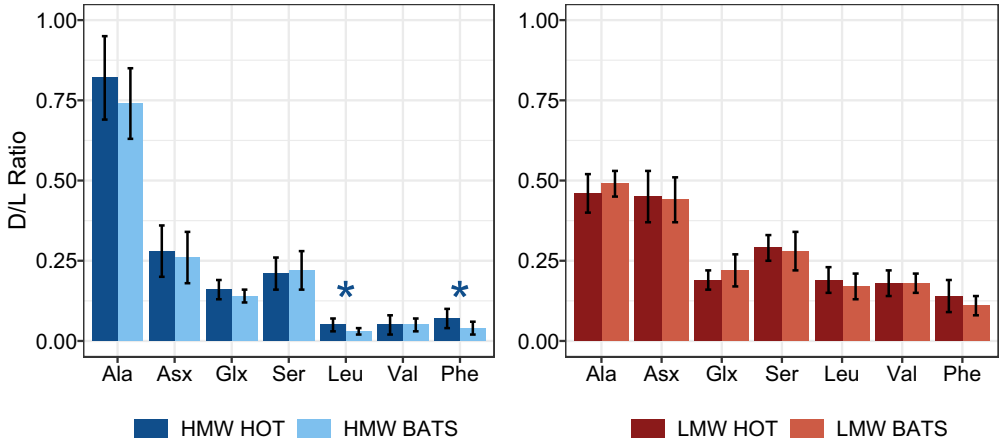

Fig. 3. Average D/L ratios of seven D-AAs measured in HMW DON (blue) and LMW SPE-DON (red) at HOT (darker shade) and BATS (lighter shade). Statistically significant differences between HOT and BATS are denoted by asterisks. Error bars represent the standard deviation of all depths and spring and summer cruise data ($n = 8$). (For interpretation of the references to colour in this figure legend, the reader is referred to the web version of this article.)

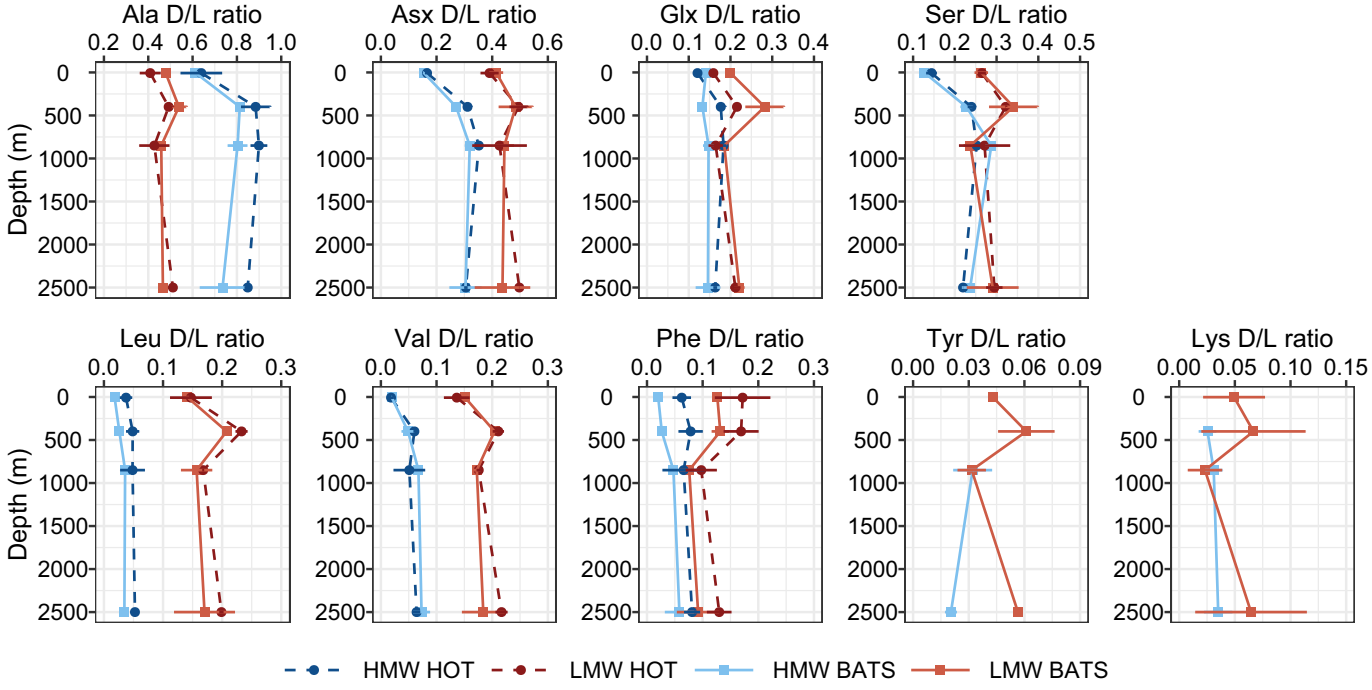

Fig. 4. D/L ratio depth profiles of four commonly reported (top row) and five newly confirmed (bottom row) D-AA. Depth trends of all D/L ratios were similar between HOT (circles, dashed line) and BATS (squares, solid line) for both HMW DON (blue) and LMW SPE-DON (red). In the LMW SPE-DON size fraction, the maximum D/L ratio is almost always observed at 400 m depth. Error bars represent the mean deviation of summer and spring cruise data and are smaller than symbol where not visible. Tyr and Lys were not measured at HOT (see Section 3.4); other missing values indicate where D-AA was indistinguishable from blank values. (For interpretation of the references to colour in this figure legend, the reader is referred to the web version of this article.)

D/L ratios and AA molar composition were also determined in the bulk UF permeate, directly representing the total LMW DON pool (Figs. S2, S3, S4). Notably, for the sampling reasons discussed in Section 2.1, as well as low natural abundance concentrations of AA in the permeate, only general trends in these data are discussed here (see Supplementary 3.0 for a more detailed discussion). D/L ratios in the UF permeate were generally similar or greater than D/L ratios of LMW SPE-DON for the same sites/depths (Fig. S3). However, the D/L ratios of UF permeate were far more variable with depth compared to the very consistent D/L ratios of LMW SPE-DON and HMW DON isolates (Fig. S3, Fig. 4). Additionally, the mean deviations of measurements made on two separate cruises were much greater in the permeate than was observed in either size fraction (Fig. S3). This variability is likely due to low concentrations of D-AA in the UF permeate, as differences in D-AA concentrations equivalent to our limit of detection for this method would translate into large differences in D/L ratios.

The overall AA molar composition of LMW SPE-DOM and the UF permeate was also very similar at all stations and depths (Figs. S2, S4). The differences in depth averaged molar abundance of individual AA between SPE-DOM and total permeate ranged from 0.0% to 5.6%, with an average molar difference of ±1.4% across all samples at HOT and BATS. Statistically significant differences in LMW SPE-DON versus permeate AA molar abundance were observed almost exclusively in AA with the lowest abundances, suggesting increased analytical error linked to low concentrations (Supplementary 3.0).

3.5. Relative molar abundance vs. D/L ratio

The average mol% and D/L ratio of each individual AA were significantly and linearly related in HMW and LMW SPE-DON at HOT and BATS (r^2 = 0.99–0.88, $p < 0.0001$–0.0017) (Fig. 5). In both HMW and LMW SPE-DON, there was no statistically significant difference in slope (ANCOVA: HMW $p = 0.39$ LMW $p = 0.71$) or y-intercept (ANCOVA: HMW $p = 0.36$, LMW $p = 0.45$) of the linear regressions between HOT vs. BATS. The slope of the linear regression of all HMW DON samples was not statistically different than the slope of all LMW SPE-DON samples (ANCOVA, $p = 0.15$). However, the y-intercept of the HMW DON linear regression was significantly lower than the y-intercept of the LMW SPE-DON linear regression (ANCOVA, $p < 0.001$).

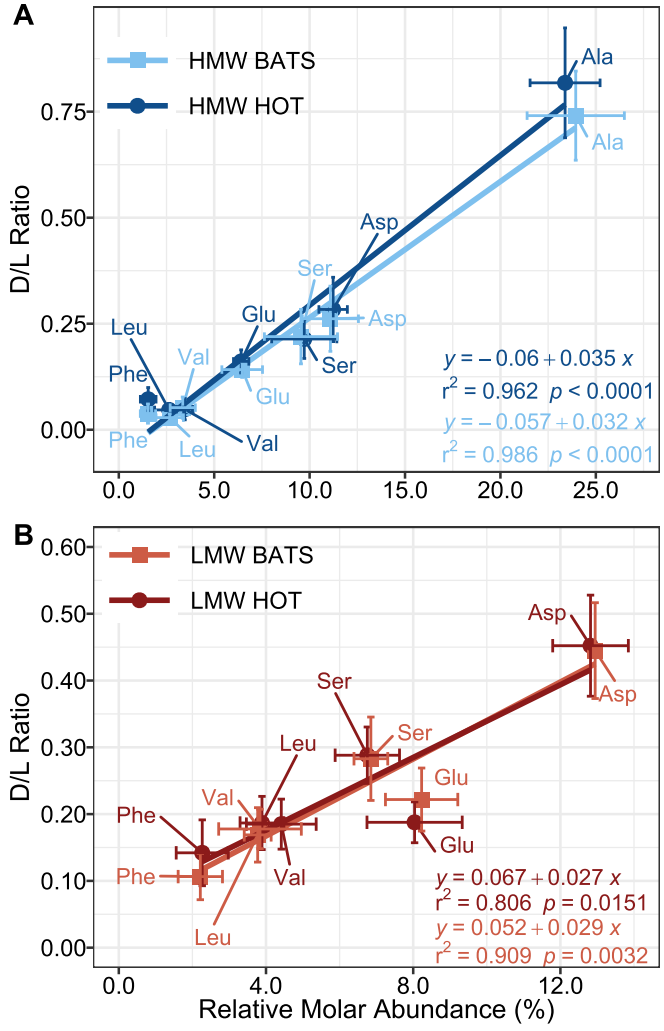

Fig. 5. Average D/L ratio and average percent relative molar abundance of individual AA were significantly linearly correlated in both (A) HMW and (B) LMW SPE-DON. For both size fractions, slope and y-intercept of linear regressions were not statistically different at HOT vs. BATS. Error bars represent the standard deviation of all HMW or LMW samples measured in that ocean basin (n = 8).

3.6. Degradation state and reactivity of HMW and LMW SPE-DON

Within each ocean basin, most AA-based degradation or bacterial source proxies were significantly different between HMW DON and LMW SPE-DON (Fig. 6, Table S3). However, individual parameters varied in their predictions for HMW versus LMW in terms of degradation state. Due to the opposite trend universally observed for D-Ala compared to all other D-AA between MW fractions (Section 3.4), total %D was calculated without D-Ala, which we refer to as $\%D_{NA}$. $\%D_{NA}$ and the combined relative mol% of β-Ala and γ-Aba, the two measured NPAA, were greater in LMW SPE-DON than HMW DON at almost all depths in both ocean basins. The organic carbon normalized total hydrolysable AA yield (%C-AA) was significantly higher in HMW DON than LMW SPE-DON at all depths. Collectively, these proxies all indicate LMW SPE-DON is less labile and more degraded than HMW DON, likely resulting in a higher relative proportion of bacterially produced biomolecules.

In contrast, %D-Ala was greater in HMW DON than LMW SPE-DON at all depths (Fig. 6), indicating a greater proportion of D-Ala containing bacterial molecules in the HMW DON pool. Additionally, no significant differences in DI were observed between HMW and LMW SPE-DON in either ocean basin. Both size fractions had the *highest* DI values (indicating the *least* degradation) at the surface, though trends with depth were variable. The $\delta^{15}N$ -based ΣV parameter values were also significantly higher (indicating *more* bacterial resynthesis) in HMW DON than in LMW SPE-DON throughout the water column at both HOT and BATS. Together, these parameters would indicate either comparable or less bacterial resynthesis and degradation to LMW DOM.

Overall, when compared within each size fraction, most AA-based proxies were very similar between ocean basins (Fig. 6). The only exceptions include %C-AA and the ΣV parameter in the HMW DON size fraction: %C-AA of HMW DON was significantly greater at HOT than BATS throughout the water column, while HMW DON ΣV was greater (indicating more bacterial resynthesis) at HOT than BATS at all depths below the surface.

PCA of AA-based proxies and D/L-ratios was used to synthesize and visualize compositional and degradation state differences between samples (Fig. 7). The first principal component (PC1) explained 73.9% of the variance and PC2 explained 13.2% of the variance. PC1 had the largest positive contributions from D/L-Val, Mol % Gly, %NPAA, D/L-Leu, D/L Asx and $\%D_{NA}$ and largest negative contributions from %C-AA, L-AA yield, and D-AA yield (Fig. 7A). The contribution of each of these indices to PC1 was ≥8%, collectively accounting for 78% of the variance along PC1. PC2 had the largest positive contributions from D/L-Ala and D/L-Ser and largest negative contribution from DI. Together, these indices contributed 83% of the variance along PC2. HMW and LMW SPE-DON were clearly separated along PC1 (Fig. 7B). Surface and deep HMW DON were separated clearly along PC2, while surface and deep LMW SPE-DON grouped together. There was no clear separation of HMW or LMW SPE-DON samples from Pacific versus Atlantic (HOT versus BATS) at any depth.

The degradation proxies which could be calculated from HPLC data alone ($\%D_{NA}$, but only including D-Asx, D-Glx, and D-Ser, total %NPAA, Mol% Gly, %C-AA, %D-Ala, and DI) were also calculated for the UF permeate (Fig. S5). Overall, the magnitude and depth trends of most degradation proxies were similar within error between LMW SPE-DON and the UF permeate (Supplementary 3.0).

3.7. Relationship between degradation indices, %D, and radiocarbon

To investigate long-term changes in AA composition and reactivity in the DON pool with age, degradation indices were plotted against $\Delta^{14}C$ values of these same MW isolates reported previously (Broek et al., 2017, 2020) (Fig. 8). In HMW DON, most measures of degradation were significantly correlated with $\Delta^{14}C$. $\%D_{NA}$, %NPAA, and mol% Gly were all significantly negatively correlated with $\Delta^{14}C$, indicating an *increase* in these bacterial biomolecules with increasing radiocarbon age of total DOM ($p < 0.001$). Similarly, DI and %C-AA were significantly positively related with radiocarbon age in HMW material, indicating an *increase* in degradation (as recorded by DI and a decrease in total AA yield) with increasing radiocarbon age ($p = 0.0028$ and $p = 0.0268$, respectively). However, all these relationships all appear driven by the large offset between surface and subsurface ($\geq$ 400 m) samples; if the surface samples are not included, only the relationship between $\Delta^{14}C$ and mol% Gly is still significant (Fig. S6).

In contrast, in the LMW SPE-DON size fraction there are fewer significant correlations between degradation indices and $\Delta^{14}C$ (Fig. 8). $\Delta^{14}C$ was significantly and positively correlated with %C-AA and with D-AA yield ($p = 0.0022$ and $p = 0.0144$, respectively), indicating a *decrease* in reactivity and an increase in bacterial degradation (total AA yield), yet also a *decrease* in bacterial source (D-AA yield) with increasing radiocarbon age. Mol% Gly was also significantly negatively correlated with $\Delta^{14}C$, indicating an increase in bacterial source or degradation with increasing radiocarbon age ($p = 0.0079$). Finally, only %NPAA was significantly positively correlated with $\Delta^{14}C$ in subsurface ($\geq$ 400 m) samples, indicating a decrease in these molecules produced via bacterial degradation with increasing radiocarbon age (Fig. S6).

4. Discussion

4.1. Total hydrolysable amino acid concentrations at HOT and BATS

The L- and D-AA concentrations of total hydrolysable AA reported in this study (Fig. 1) are comparable to those reported previously at BATS and HOT (Kaiser and Benner, 2008). Earlier reports of L-AA concentrations at both BATS versus HOT are limited and suggest more variable concentrations (Lee and Bada, 1977; McCarthy et al., 1996). At the surface, the higher hydrolysable AA concentrations at HOT reported here and by Kaiser and Benner (2008) suggest either greater surface AA production or greater resistance of labile biochemicals compared to surface waters at BATS. At 2500 m depth, in contrast, the AA concentrations are similar or greater at BATS than HOT (see Supplementary 1.0), a trend also documented by Kaiser and Benner (2008) and consistent with more extensive microbial removal of labile biomolecules in the older Pacific mesopelagic ocean waters.

4.2. D-AA and bacterial source of DON at HOT and BATS

We report here an expanded suite of D-AA in HMW and LMW SPE-DON. Only four D-AA (D-Ala, D-Asx, D-Glx, and D-Ser) have been commonly reported in most past marine DOM literature (Kaiser and Benner, 2008; McCarthy et al., 1998; Shen et al., 2017). Two additional D-AA, D-Leu and D-Val, have been reported in coastal and terrigenous DOM, however at near-blank levels (Bourgoin and Tremblay, 2010; Hébert and Tremblay, 2017; Tremblay and Benner, 2006). Recently, D-Leu, D-Val, and D-Phe were confirmed for the first time in open ocean DOM based on large samples coupled with mass spectral verification (Broek et al., 2019). This study expands observations of these new D-AA

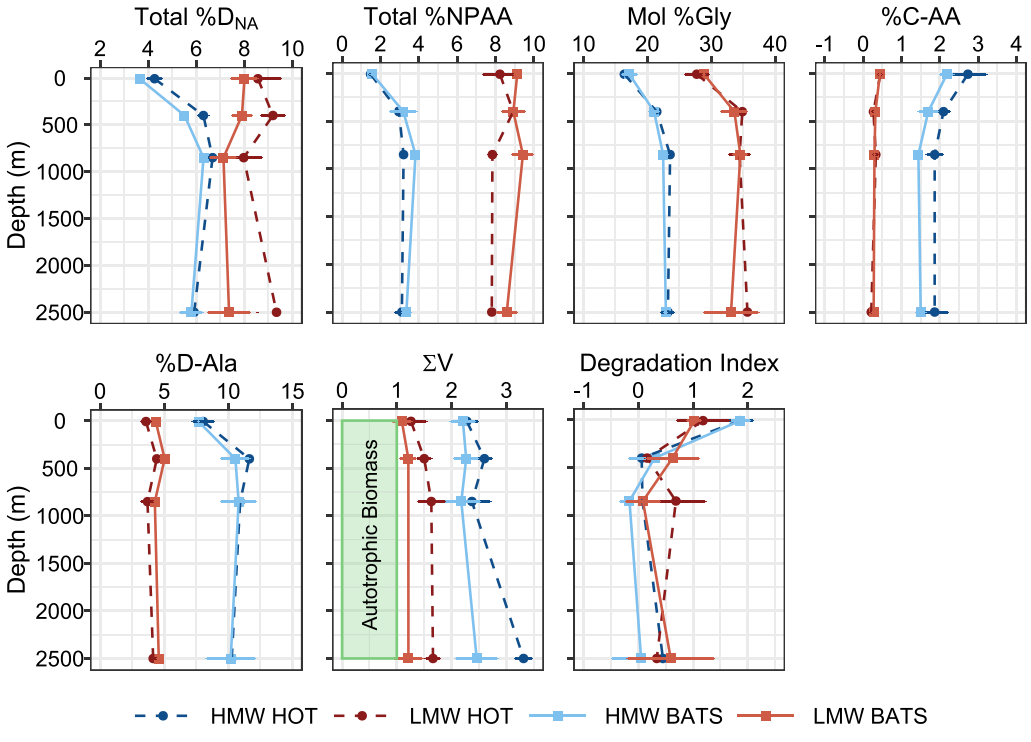

Fig. 6. Depth profiles of common AA-based proxies in HMW DON (blue) and LMW SPE-DON (red) at HOT (circles, dashed line) and BATS (squares, solid line). %D without D-Ala ($\%D_{NA}$), total % non-protein AAs (NPAA), mol% Gly, and %C-AA (top row) all indicate lower reactivity, greater bacterial source contribution or greater bacterial degradation to LMW SPE-DON compared to HMW DON. In contrast, %D-Ala, ΣV, and DI (bottom row) all indicate similar or greater bacterial source, resynthesis, and degradation in HMW DON versus LMW SPE-DON. Error bars represent the mean deviation of summer and spring cruise data for all proxies except ΣV. Because ΣV could only be measured on spring cruise data, error bars represent the propagated analytic error associated with triplicate isotopic measurements of each AA. For all proxies, error bars smaller than symbol were not visible. (For interpretation of the references to colour in this figure legend, the reader is referred to the web version of this article.)

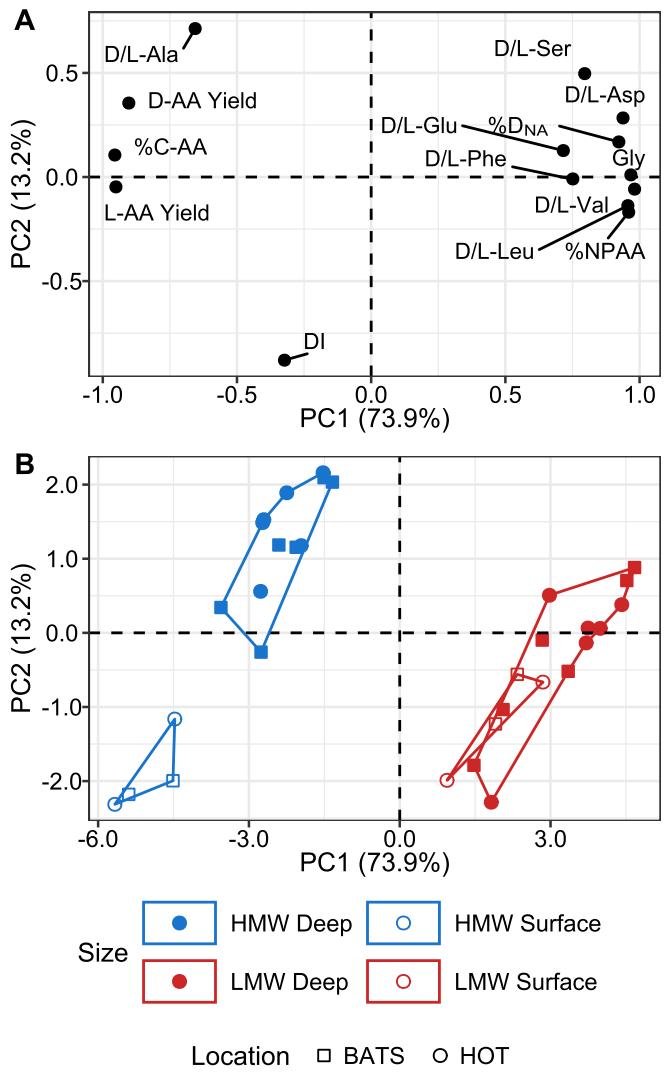

Fig. 7. Principal component analysis (PCA) of AA-based proxies and D/L ratios of HMW DON (blue) and LMW SPE-DON (red) from BATS (squares) and HOT (circles). (A) Loadings of D/L ratios and degradation indices. Only variables that were measured in all samples are included in the PCA. (B) PCA scores show clear separation of HMW and LMW SPE-DON. Surface (open symbols) HMW DON is clearly separated from deep (filled symbols) HMW DON while surface LMW SPE-DON groups with deep LMW SPE-DON. (For interpretation of the references to colour in this figure legend, the reader is referred to the web version of this article.)

to the Atlantic Ocean (BATS site) while further identifying two additional D-AA (D-Lys and D-Tyr), which to our knowledge have never been reported in any natural water. Our data indicate that D-AA within this greatly expanded suite of bacterial tracers falls into distinct groupings based on abundance and relative concentrations changes in HMW and LMW material.

All recently identified D-AA (D-Leu, D-Val, D-Phe, D-Tyr, D-Lys) are more abundant in LMW SPE-DON than HMW DON at both HOT and BATS. The significantly greater D/L ratios of D-Leu, D-Val and D-Phe in LMW SPE-DON compared to HMW DON in both ocean basin (Section 3.4, Figs. 3, 4) support previous work which hypothesized that these D-AA may be tracers specific for refractory bacterial AA containing-molecules (Broek et al., 2019). Similarly, our PCA indicated that of the seven most abundant D-AA measured in every sample (excluding D-Tyr and D-Lys), D/L-Leu and D/L-Val had the greatest positive contributions to PC1, associated with the ^{14}C-old LMW SPE-DON fraction (Fig. 7). Although D-Tyr and D-Lys could not be confirmed above blank values in all our HMW DOM samples, the D/L ratios of these two D-AA in LMW SPE-DON had very similar depth structure to the other newly identified or confirmed D-AA (Fig. 4). While mass spectral data confirm authentic compounds, these consistent oceanographic depth trends provide further confidence that these D/L ratios represent natural compounds. Together, these observations suggest that D-Tyr and D-Lys may have similar sources as other newly identified D-AA.

In contrast to all other D-AA, D-Ala was the only D-AA with a greater D/L ratio in HMW DON than in LMW SPE-DON, also consistent with previous work (Broek et al., 2019; Kaiser and Benner, 2008) (Figs. 3, 4, Table S4). Similarly, PCA analyses indicates D/L-Ala is the only D/L ratio associated with HMW DON rather than LMW SPE-DON (Fig. 7). Together, this suggests D-Ala traces unique, more labile, bacterial products. D-Ala is a key component of both autotrophic and heterotrophic bacterial peptidoglycan (Cava et al., 2011; Kaiser and Benner, 2008; Schleifer and Kandler, 1972), a HMW polymer which is hydrolyzed relatively rapidly in seawater (Jørgensen et al., 2003; Nagata et al., 2003). Our data are therefore consistent with past work suggesting that D-Ala could mostly trace bacterial peptidoglycan (Broek et al., 2019). However, we note that D-Ala is also found in other bacterial compounds besides peptidoglycan (Kaiser and Benner, 2008; Schleifer and Kandler, 1972), meaning other D-Ala containing molecules cannot be ruled out. Regardless, because D-Ala uniquely accumulates in HMW DON and appears to trace more labile compounds compared to all other D-AA, we suggest %D-Ala should be reported and considered separately in future DOM data. In the text below, we therefore exclude D-Ala in discussion of the percentage of total D-AA (%D_{NA}).

While the AA composition of HMW versus LMW DON was clearly distinct, the AA composition within both size fractions was remarkably similar between BATS And HOT. The nearly identical depth profiles of D/L ratios and relative mol% contributions at HOT and BATS within each size fraction (Fig. 4, Fig. S2) suggest that very similar microbial sources and removal processes define the composition of AA-containing material at similar depths throughout both ocean basins. This conclusion is also supported by the strong, apparently universal linear relationships between average D/L ratios and molar abundance in both HMW and LMW SPE-DON ($r^2 = 0.88$ to 0.99, $p < 1 \times 10^{-4}$ to 0.0017) which are not statistically different between the two ocean basins (Fig. 5) (Broek et al., 2019). These relationships directly show that in both size fractions the most abundant chiral AA were also those with the highest bacterial contributions (as indicated by D/L ratio). While we are unsure what the y-intercept represents, the difference in y-intercept between HMW DON and LMW SPE-DON might reflect the different D-AA composition of these two size fractions. Still, the similar slopes indicate an almost identical progression of D-AA composition with total AA abundance, and overall suggest that bacterially produced AA may dominate the entire dissolved AA pool.

Finally, while theoretically it is possible that abiotic racemization could contribute to D-AA accumulation in our samples, it is unlikely this would create the D-AA distributions observed in our data. While abiotic racemization of AA does occur over millennial timescales, these rates are too slow to account for the high D/L ratios we observed (Bada, 1971). For example, Phe has the fast abiotic racemization rate of those published in Bada (1971), and one of the lowest D/L ratios in our data, yet in our oldest sample ($\Delta^{14}C = 6860$ yr BP), abiotic racemization would yield D/L ratio for Phe an order of magnitude less than what we measured (0.015 versus 0.15). In addition, an abiotic source would be expected to produce a far more regular distribution based on only on relative racemization rate and could not explain the oceanographically distinct profiles. Given that past work has shown that heterotrophic bacteria can produce all the D-AA we report in this study (Azúa et al., 2014; Cava et al., 2011; Lam et al., 2009; Zhang et al., 2016), together this provides support that bacteria are the major producers of D-AA in both HMW and LMW DON.

Together, these observations suggest that within each size fraction similar bacterial processes have utilized and resynthesized most

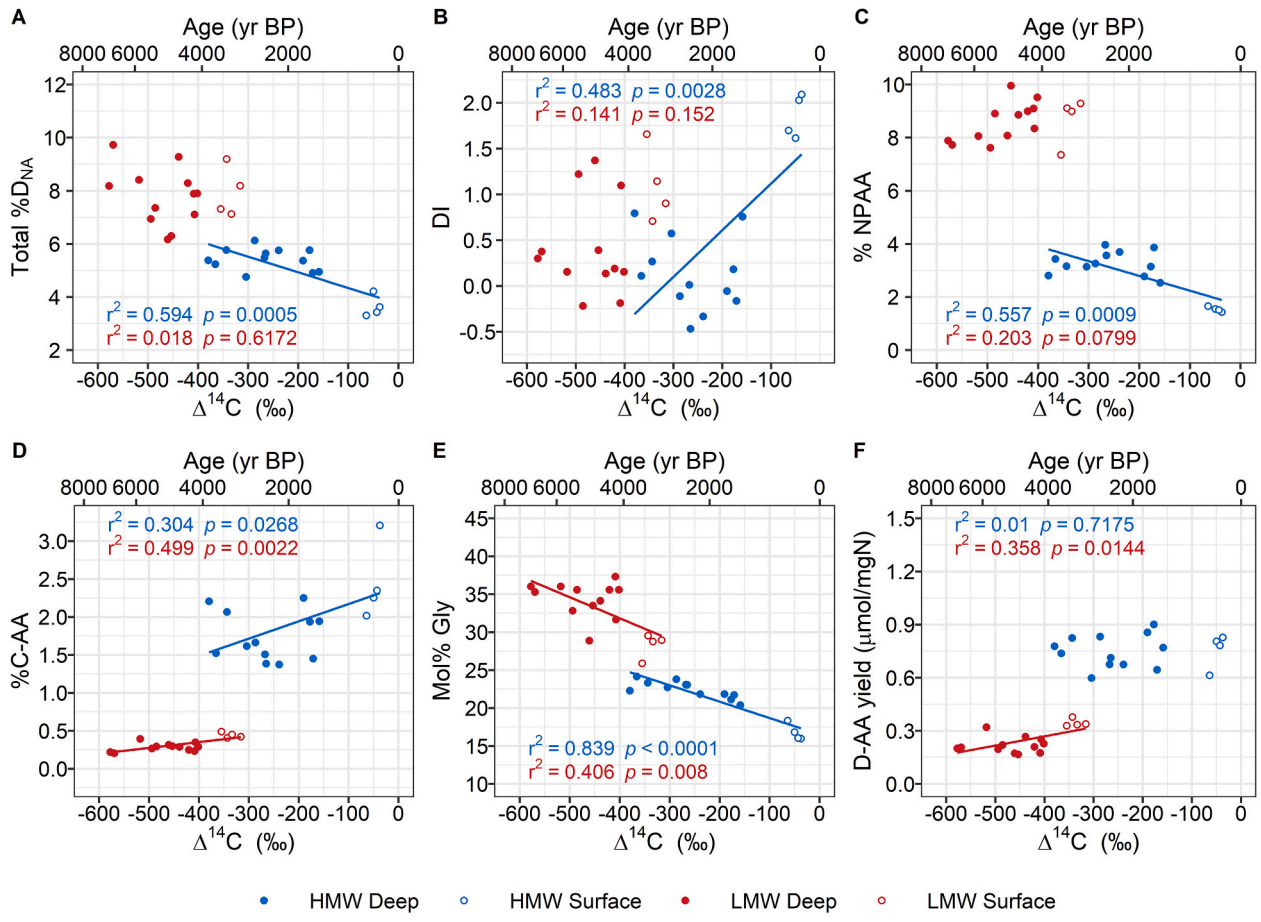

Fig. 8. Linear regressions of common AA-based proxies vs. $\Delta^{14}C$: (A) $\%D_{NA}$ (excluding D-Ala), (B) Degradation Index (DI), (C) % non-protein amino acids (NPAA), (D) %C-AA (E), mol% Gly, and (F) total D-AA yield (μmol/mgN). HMW DON and LMW SPE-DON include data from both HOT and BATS, with significant linear regressions indicated by solid regression lines. Almost all indices have significant regressions with $\Delta^{14}C$ in HMW DON (blue) when surface samples (open circles) are included, though most relationships are no longer significant in only subsurface samples (≥ 400 m, filled circles) (Fig. S6). In contrast, few relationships are significant in LMW DON (red) with or without surface samples (Fig. S6). Upper x-axis represents approximate age in years before present (BP) calculated from radiocarbon Δ notation values according to: Age = 8033*ln(1+ $\Delta^{14}C$/1000). (For interpretation of the references to colour in this figure legend, the reader is referred to the web version of this article.)

eukaryotic algal material at both BATS and HOT, while refractory D-AA containing molecules are selectively preserved. These processes result in remarkably similar D and L-AA composition when comparing the two sites and could imply that AA-containing molecules in the subsurface of both size fractions are relatively refractory. Yet, at the same time, the composition of bacterial products appears to be clearly distinct between the HMW and LMW SPE-DON pools. Overall, this suggests a difference in bacterial sources and production of HMW versus LMW SPE-DON material, potentially indicating unique bacterial sources for the most long-lived DON.

4.3. Potential diversity of D-AA containing molecules

In contrast to the individual D/L-AA ratios (i.e., μmol D-AA normalized to μmol L-AA), which are specific to AA-containing molecules, the total D and L-AA yields (μmol D or L-AA normalized to mg total organic nitrogen) provide information regarding the composition and bacterial contribution to total DON (Table S1). Specifically, the L-AA yield is often used as an indicator of reactivity, with a higher L-AA yield indicating a greater proportion of the total ON is made of supposedly labile L-AA (Davis et al., 2009; Kaiser and Benner, 2009). In contrast, D-AA yields represent the relative proportion of total DON which is bacterially derived, with a higher D-AA yield indicating greater bacterial contribution (Bourgoin and Tremblay, 2010; Kaiser and Benner, 2008; Tremblay and Benner, 2006, 2009). While the D-AA yields of individual AA in total DOM are often used to quantify the percent of bacterial DOC or DON, extremely variable and unreasonable (> 100%) results were observed for total, HMW, and LMW SPE-DON (Fig. S7). We suggest this is likely due to the lack of bacterial biomarker endmembers specific for HMW and LMW SPE-DON, as well as several assumptions of this calculation which could result in inaccurate values if not met (Supplementary 4.0). Still, a comparison of D and L-AA yield trends with depth can be informative about the reactivity of AA-containing molecules in both size fractions.

One major implication from the D-AA and L-AA yields is that D-AA present in HMW and LMW SPE-DON appear to have not only different compositions, but also very different reactivities compared to total ON in each size fraction. This would also be consistent with D/L ratio data discussed above. An earlier bacterial degradation study suggested that the four common D-AA (D-Ala, D-Glx, D-Ser, and D-Asx) all have similar reactivity to total bacterial DON (Kawasaki and Benner, 2006). However, bacterial incubations which included some newly identified D-AA indicated greater bioavailability of "canonical" D-AA (D-Ala, D-Asx, D-Glx) which are all abundant in HMW material, vs. "non-canonical" D-AA (D-Leu, D-Met, D-Val) (Wang et al., 2020), which are more abundant in our LMW material. Additionally, recent work investigating marine DOM

D/L ratios with radiocarbon age also indicated varying reactivity of compounds containing D-Ala, D-Glx, D-Ser, and D-Asx versus D-Leu, D-Val, and D-Phe overall longer timescales (Broek et al., 2019). The difference in D-AA yield depth trends in HMW versus LMW SPE-DON reported here confirm and expand this idea (Fig. 2), implying a difference in the lability, and likely also in molecular composition, of D-AA containing compounds in HMW versus LMW SPE-DON.

In HMW DON, the consistent or increasing D-AA yield in the upper ocean suggests HMW D-AA containing compounds are *more* refractory than total HWW DON, while decreasing L-AA yields indicate L-AA containing compounds are preferentially removed. This is further supported by the greater D-AA yield at HOT compared to BATS, which indicates greater persistence of D-AA containing compounds compared to total ON in the older waters at HOT. These observations are also consistent with the increase in D/L ratios of some AA with depth in HMW DON (Ala, Asx, Ser, Val, Fig. 4), suggesting removal of L-AA compared to D-AA, as well as with the general expectation that D-AA containing biomolecules are less labile than their L-AA counterparts.

In contrast to the HMW DON pool, the coupled decreases in both L- and D-AA yields with depth in the LMW SPE-DON pool indicate that both L- and D-AA containing compounds are preferentially utilized compared to total LMW SPE-DON (Fig. 2). At the same time, the maximum D/L ratios observed at 400 m for nearly every LMW D-AA in both ocean basins (Fig. 4) imply a relative accumulation of LMW bacterially sourced molecules in the mesopelagic. Based on similar observations at HOT, Broek et al. (2019) suggested an input of fresh, heterotrophic bacterial material to the mesopelagic ocean. While exact processes leading to these maxima are beyond the scope of this study, it seems clear that unique processes are shaping the D-AA composition of LMW SPE-DON and HMW DON pools, and that these appear to have clear water column structure.

These observations may have important implications for how we understand the nature of AA containing DON, which are often interpreted as "proteinaceous" material. Because free AA are a very minor portion of total hydrolysable AA (Lee and Bada, 1977; McCarthy and Bronk, 2008), measurable changes in L-AA and D-AA yields reported here must be interpreted as either production or microbial degradation of L-AA and D-AA containing macromolecules. However, the consistently high concentrations of many bacterial D-AA, coupled with the strong and universal correlations to L-AA distributions (Fig. 5), at least suggest non-proteinaceous bacterial sources. This would also be consistent with the relative reactivity of HMW and LMW SPE-DON D-AA that we observed, indicating different dominant D-AA containing compound classes in these two size fractions. For example, we would expect proteinaceous material (larger peptides and partially degraded protein fragments) and larger fragments of structural compounds (such as peptidoglycan), to be retained in our HMW size fraction (> 2.5 kDa). In contrast, compounds isolated in our LMW SPE-DON size fraction are more likely to either be less-labile, smaller, AA-containing natural products or else fragments of larger biomolecules (discussed further in Section 4.4.2). Together with the results above, such considerations suggest the differing reactivities of D-AA containing compounds in HMW DON and LMW SPE-DON are linked to distinct biomolecule compositions, and since D-AA are not found in proteins, in turn that many may not be "proteinaceous." For example, lipopeptides, siderophores, pigments, and bacterial signaling molecules can all have both D and L-AA (Asano and Lübbehüsen, 2000; Cava et al., 2011; Kaiser and Benner, 2008; Radkov and Moe, 2014; Schleifer and Kandler, 1972). Further, the role of many D-AA produced by bacteria remains unknown, meaning there are also likely multiple additional D-AA containing molecule classes which remain to be characterized (Radkov and Moe, 2014).

4.4. Degradation signatures of HMW and LMW SPE-DON: Bacterial source or progressive degradation?

4.4.1. Correlations with $\Delta^{14}C$: Progressive bacterial degradation of HMW DON?

To explore potential bacterial alteration over ocean mixing timescales, we investigated relationships between AA-based proxies and $\Delta^{14}C$. If bacterial alteration of HMW DON with ocean circulation is progressive, as opposed to simply occurring in the biologically most active surface zone, then we would expect degradation parameters to correlate with $\Delta^{14}C$. While total DOM $\Delta^{14}C$ likely does not exactly represent the $\Delta^{14}C$ of DON, the $\Delta^{14}C$ of protein-like HMW material indicates it is at least a reasonable proxy (Loh et al., 2004). The strong relationships observed between almost all AA-based proxies and $\Delta^{14}C$ in the HMW DON pool would seem to validate using bulk $\Delta^{14}C$ ages, and to indicate that bacterial degradation is progressively changing surface produced HMW DON with radiocarbon age on millennial timescales (Fig. 8). Only the D-AA yield (in contrast to $\%D_{NA}$) is not significantly correlated with $\Delta^{14}C$, suggesting that changes to AA composition in this size fraction are due to net *removal* of L-AA rather than addition of D-AA. These full water column data therefore seem to suggest a continuous and progressive degradation of HMW DON over >3500 years of DOM age, with bacteria selectively removing labile L-AA from HMW DON, while also changing the relative mol % contribution of AA (DI) and increasing the relative proportion of refractory D-AA, Gly, and the NPAA in HMW DON.

However, consideration only of deeper data (for samples between 400 m and 2500 m) completely changes this interpretation, as most of the same proxies no longer have any relationship with $\Delta^{14}C$ (Fig. S6). Additionally, PCA of D/L ratios and degradation proxies indicate surface HMW DON has a distinct composition from all subsurface (≥ 400 m) samples (Fig. 7B). Considering the expected relative lability of proteinaceous HMW DON (Amon et al., 2001; Amon and Benner, 1996), the lack of further changes to AA composition with age beyond the mesopelagic (representing a radiocarbon age difference > 2000 years between mesopelagic and deep waters at HOT) might be seen as surprising. However, it appears that by the time advected HMW DON reaches mid-thermocline depths, AA-containing molecules remaining are relatively stable and undergo little further compositional change with time. Only the ΣV offset in deep waters between the ocean basins would seem to contradict this, although this offset is only based on a few data points. Still, this could potentially suggest that if continuing slow bacterial remineralization is the main mechanism for this older HMW DON, CSI-AA patterns alone would reflect this process in very old DOM.

Overall, for HMW DON, these results are generally consistent with a "two-pool" model; reactive semi-labile HMW DON appears produced and then restricted to the upper water column, while an additional "background" HMW DON pool appears to be relatively refractory and unchanging in mesopelagic and deep ocean. This is consistent with radiocarbon measurements of "protein-like" HMW DON, estimating this material to be 3000–4000 years old (Loh et al., 2004). Additionally, a similar concept was proposed based on solid-state NMR results, which suggested HMW DON is composed of two chemically distinct pools with varying reactivities (Aluwihare et al., 2005). If almost all HMW DON is in fact proteinaceous material (Aluwihare et al., 2005; McCarthy et al., 1997), these results would further imply bacterial alteration of proteinaceous material produces stable compounds which can persist for thousands of years. Indeed, the observation that most AA-based degradation proxies behave in similar, expected ways in the HMW DON fraction may itself be further evidence for a predominantly proteinaceous N pool in HMW material.

4.4.2. Direct surface bacterial source of LMW SPE-DON?

The discrepancies between degradation state of LMW SPE-DON as predicted by different degradation parameters suggests a disconnect in how individual parameters reflect "degradation" in this size fraction

(Fig. 6). As noted above (Section 3.6), most parameters linked to D or L-AA yields indicated increased degradation or bacterial source in the LMW SPE fraction when compared to the HMW fraction at all depths (% D_{NA}, %NPAA, mol% Gly, and %C-AA), consistent with expectations based on older average radiocarbon ages for this size fraction. However, in contrast, the $\delta^{15}N$-based ΣV parameter indicated *less* bacterial resynthesis in LMW SPE-DON at all depths compared to HMW DON, with values close to what would be expected from autotrophic production. Additionally, the substantially lower %D-Ala and similar DI values compared to HMW DON indicated equivalent or less bacterial degradation to LMW SPE-DON (Fig. 6). We suggest a few possible interpretations consistent with the data reported here, which we note are not mutually exclusive.

One is the potentially different composition of LMW AA-containing molecules hypothesized above (Section 4.3). If substantial LMW nitrogenous material is in fact bacterial, but not proteinaceous, then the "baseline" levels of many degradation parameters might be very different in comparison with proteinaceous N which dominates HMW material. This possibility is supported by a lack of significant relationships between %D-Ala and $\%D_{NA}$ versus DI in the LMW SPE-DON size fraction, which suggests DI does not record bacterially mediated changes in this material (Supplementary 5.0, Fig. S8). As noted above, unique biomolecular sources of D-AA containing compounds in LMW SPE-DON would also be consistent with previous work reporting D-AA content in the LMW DON pool (Broek et al., 2019; Kaiser and Benner, 2008).

A second possibility is that patterns of D-AA, NPAA, and most AA yields in LMW SPE-DON reflect well preserved bacterial source signatures, irrespective of composition, which are created in the surface ocean and then undergo little subsequent bacterial alteration even on millennial timescales. Production of refractory, LMW DOM can occur via direct bacterial release during growth or viral lysis (Gruber et al., 2006; Ogawa et al., 2001), consistent with LMW D-AA potentially representing a "fresh" bacterial source signal. In this scenario, bacterial production would produce LMW molecules with inherently lower L-AA yields (and lower %C-AA) and a greater contribution of bacterially derived molecules (D-AA and NPAA), compared to HMW molecules. This interpretation would be most consistent with the low ΣV values, which are all close to ranges for autotrophic algae (Section 2.9, McCarthy et al., 2007). The limited relationships between $\Delta^{14}C$ values and bacterial proxies in LMW SPE-DON further support this idea (Fig. 8), and could imply that at least D-AA, DI and NPAA are a predominantly a surface bacterial source signature. Indeed, the significant decrease in D-AA yield with $\Delta^{14}C$ in the LMW SPE-DON (Fig. 8f), is the opposite of what would be expected if the relative D-AA contribution in this material were increasing with age. Similarly, PCA of AA-based proxies shows no separation of LMW SPE-DON samples by depth or ocean basin, indicating all LMW SPE-DON samples investigated here have a similar composition and degradation state everywhere we sampled in the ocean (Fig. 7). Together, these data support the idea that D-AA in LMW SPE-DON could be predominantly an indicator of refractory bacterial AA-containing molecules produced in the surface ocean, with no real impact from further progressive heterotrophic degradation or resynthesis.

Finally, it is important to note, however, that the depth and sampling limitations inherent in these data do not tightly constrain the timescales of these processes. Even the youngest HMW material isolated from the surface has average $\Delta^{14}C$ ages of hundreds of years, while the LMW material is far older, by mass balance representing a mixture of newly produced LMW SPE-DON and refractory background material. Our data set therefore suggests that in contrast to HMW DON, no major compositional changes occur in LMW SPE-DON over hundreds to thousands of years. Put another way, any alteration of LMW AA-containing molecules on decadal timescales would appear "preformed" in our sample set.

4.5. How representative is LMW SPE-DON of the total LMW DON pool?

While these data are specific only to the LMW SPE-DON isolated in this study, it is possible our data and conclusions may extend to a larger portion of the total LMW DON pool. For our AA data specifically, the similarity of the AA composition (Figs. S2, S4) and most degradation state parameters (Fig. S5) between the UF permeate and LMW SPE-DON suggests our LMW SPE-DON samples may be fairly representative of overall AA composition in total LMW DON. While D/L AA data was somewhat more variable (Fig. S3), the lack of evidence for any total AA selectivity, and the basic fact that SPE resin is non-chiral, both suggest that such offsets are due to analytical variation discussed above in low permeate D-AA concentrations. Together with the similar recoveries of total hydrolysable AA and DON in our LMW SPE size fraction (Table 1), the available data thus suggest that despite SPE recovering a relatively modest fraction of total LMW AA, the LMW SPE material is mostly *non-selective* for AA targeted here. This conclusion is also supported more broadly by bulk $\delta^{15}N$ data published previously (Broek et al., 2017) which show that total LMW DON has a very similar $\delta^{15}N$ value as LMW SPE-DON.

Therefore, while we cannot confidently say exactly to what degree these results apply to the total LMW DON pool, together these data indicate that our conclusions likely extend beyond the LMW SPE-DON material we directly isolated. The exact correspondence, however, will be key topic for future experiments. We suggest future experiments should be designed to test what portion of the total LMW DON pool is represented by LMW SPE-DON with rigorous mass and isotope mass balances for total LMW DON and the fraction which can be resin isolated. Finally, at the same time, it should be stressed that while the isolated proportion may seem modest, the directly isolated material in this study alone (HMW ultrafiltered DON and LMW SPE-DON) together makes up by far the greatest proportion of total DON and total dissolved AA ever directly investigated.

4.6. Two independent pools of DON?

Taken together, a comparison of D/L ratios, relative AA molar abundance data, and degradation state proxies for HMW and LMW SPE-DON shows clear compositional differences between these two size fractions at every depth (Figs. 4, 6, Fig. S2). PCA further indicated that HMW and LMW SPE-DON are compositionally distinct (Fig. 7). At the same time, *within* each size fraction, AA composition was remarkably similar with depth between the Atlantic and Pacific Oceans (Figs. 3, 4, 6, Fig. S2) and there was little evidence that the AA composition of either size fraction undergoes significant changes on timescales amenable by $\Delta^{14}C$ data (Fig. 8, Fig. S6). While our LMW SPE-DON only represents a subset of the total DON pool, as noted above comparisons of the AA composition and parameters with total LMW DON (via the UF permeate) and LMW SPE-DON do not indicate drastic differences.

Overall, these results may suggest a departure from current assumptions that progressive bacterial degradation produces refractory, LMW DON. Where we hypothesized an approximate continuum of degradation and D-AA composition with radiocarbon ages between the HMW and LMW SPE-DON pools, instead the distinct AA compositions we observed seem to suggest that AA compositional differences may be "preformed" in HMW and LMW material in the surface ocean. The somewhat surprising general lack of changes to DON AA composition or degradation state with $\Delta^{14}C$ data we observed in both pools supports this idea, suggesting that, at least in the subsurface ocean, AA-containing molecules in HMW and LMW SPE-DON cycle independently. While this is a hypothesis that remains to be tested, this interpretation would be consistent with previous studies specific to the DON pool, which suggested independent production and cycling of HMW and LMW DON (Broek et al., 2019; Knapp et al., 2012). Additionally, it would call into question whether the "size-age-reactivity" idea, widely applied to the DOC pool (e.g., Amon and Benner, 1994, 1996; Walker et al., 2014,

2016), could apply to DON in the same way. However, we again note that if size-continuum changes are very rapid in the surface ocean, this linkage could not be tested by $\Delta^{14}C$ data correlations and could potentially still be consistent with the separate AA compositional pools we observe. Targeted experiments measuring the evolution of all these parameters simultaneously in culture would be useful in addressing this possibility.

5. Conclusions

We report here an expanded suite of D-AA measured directly in both HMW and LMW SPE-DON at BATS. These data are interpreted in the context of existing data at HOT and are paired with DOM $\Delta^{14}C$ ages and multiple independent bacterial AA-based proxies. Our new data confirm recent observations that three novel D-AA are ubiquitous in marine DON (D-Leu, D-Val, and D-Phe). Additionally, we report two new D-AA which have never previously been reported in any natural water (D-Tyr and D-Lys). D/L ratios of all five D-AA are greater in the older, LMW SPE-DON size fraction, suggesting they may be developed as novel tracers for bacterially produced, most refractory DON molecules. The clearly distinct D-AA compositions within the HMW and LMW SPE-DON pools at all ocean depths suggest that AA containing molecules in DON are more diverse than previously believed. We hypothesize that these differences are indicative of unique D-AA containing molecules in HMW versus LMW SPE-DON, many of which may not be proteinaceous.

By coupling D-AA composition with multiple measures of bacterial source, degradation and radiocarbon age, we also evaluated how different measures of DON reactivity and degradation change over time in the HMW versus LMW SPE-DON pools. All AA-based proxies indicated heterotrophic bacterial alteration of HMW DON throughout the mesopelagic, supporting the paradigm of a surface produced, semi-labile HMW DON component which is then progressively altered by bacteria. However, in the subsurface, a lack of relationships between most AA-based proxies and $\Delta^{14}C$ indicated a "background" pool of HMW DON which appears relatively refractory.

In contrast, in the LMW SPE-DON pool, AA-based proxies yielded conflicting results regarding degradation state, with some indicating LMW SPE-DON is more refractory and degraded than HMW DON, while others indicated LMW SPE-DON is less degraded and potentially predominantly autotrophic. Additionally, in contrast to HMW DON, few significant relationships were observed between $\Delta^{14}C$ and AA-based degradation proxies. We hypothesize that together these data indicate that bacterially derived LMW AA-containing molecules produced in the surface ocean may be intrinsically more refractory, and therefore less susceptible to degradation than HMW bacterial AA-containing molecules.

Overall, the distinct L-AA and D-AA signatures of HMW and LMW SPE-DON, coupled with the consistent AA composition and degradation state parameters in the deep, older background pool of both size fractions, suggest separate pools of material. This interpretation runs counter to expectations that the AA composition of HMW DON would progressively shift towards that of LMW DON. Instead, our results indicate independent composition, sources, and cycling of AA-containing molecules in HMW and LMW SPE-DON. If true, this hypothesis would represent a paradigm shift for DON cycling, suggesting the most refractory, AA-containing compounds in LMW DON may be preformed in the surface ocean. While these results are most directly applicable to the LMW SPE-DON isolated in this study, the AA composition and degradation parameters of LMW SPE-DON and total LMW DON (UF permeate) were similar, indicating that these conclusions may apply to a greater portion of the total LMW DON pool than we directly isolated here. Finally, our data also support a growing body of work suggesting that amide functionality in marine DON may not be limited to proteinaceous material, but likely encompasses a far more diverse range of other, currently uncharacterized, N-containing molecules. Future work identifying the composition of non-proteinaceous nitrogenous material will aid in determining potential sources and degradation processes of refractory organic nitrogen.

Supplementary data to this article can be found online at https://doi.org/10.1016/j.marchem.2022.104104.

Funding

This work was primarily supported by a grant from NSF Chemical Oceanography (Award # 1358041). Additional support was provided by the National Science Foundation Graduate Research Fellowship Program (to H.I.), the National Natural Science Foundation of China (NSFC) (42106040 to Y.S.) and the Fundamental Research Funds for the Central Universities of China (20720210076 to Y.S.).

Declaration of Competing Interest

The authors declare that they have no known competing financial interests or personal relationships that could have appeared to influence the work reported in this paper.

Acknowledgments

The authors thank the captains and crews of the UNOLS vessels R/V *Kilo Moana* and R/V *Atlantic Explorer* for assistance with collection of this novel sample set. We also thank Stephanie Christensen for assistance with GC–MS protocols and Ronald Benner for providing the facility for HPLC amino acid analysis. Finally, we thank two anonymous reviewers for feedback which improved the manuscript.

References

Aluwihare, L.I., Repeta, D.J., Pantoja, S., 2005. Two chemically distinct pools of organic nitrogen accumulate in the ocean. Science 308. https://science.sciencemag.org/content/308/5724/1007/tab-pdf.

Amon, R.M.W., Benner, R., 1994. Rapid cycling of high-molecular-weight dissolved organic matter in the ocean. Nature 369 (6481), 549–552. https://doi.org/10.1038/369549a0.

Amon, R.M.W., Benner, R., 1996. Bacterial utilization of different size classes of dissolved organic matter. Limnol. Oceanogr. 41 (1), 41–51. https://doi.org/10.4319/lo.1996.41.1.0041.

Amon, R.M.W., Fitznar, H.-P., Benner, R., 2001. Linkages among the bioreactivity, chemical composition, and diagenetic state of marine dissolved organic matter. Limnol. Oceanogr. 46 (2), 287–297. https://doi.org/10.4319/lo.2001.46.2.0287.

Asano, Y., Lübbehüsen, T.L., 2000. Enzymes acting on peptides containing D-amino acid. J. Biosci. Bioeng. 89 (4), 295–306. https://doi.org/10.1016/S1389-1723(00)88949-5.

Azam, F., Fenchel, T., Field, J.G., Gray, J.S., Meyer-Reil, L.A., Thingstad, F., 1983. The ecological role of water-column microbes in the sea. Mar. Ecol. Prog. Ser. 10, 257–263.

Azúa, I., Goiriena, I., Baña, Z., Iriberri, J., Unanue, M., 2014. Release and consumption of D-amino acids during growth of marine prokaryotes. Microb. Ecol. 67 (1), 1–12. https://doi.org/10.1007/s00248-013-0294-0.

Bada, J.L., 1971. Kinetics of the nonbiological decomposition and racemization of amino acids in natural waters. In: Hem, J.D. (Ed.), Nonequilibrium Systems in Natural Water Chemistry, vol. 106. American Chemical Society, pp. 309–331. https://doi.org/10.1021/ba-1971-0106.ch013.

Benner, R., 2002. Chemical composition and reactivity. In: Biogeochemistry of Marine Dissolved Organic Matter. Elsevier, pp. 59–90. https://doi.org/10.1016/B978-012323841-2/50005-1.

Benner, R., Amon, R.M.W., 2015. The size-reactivity continuum of major bioelements in the Ocean. Annu. Rev. Mar. Sci. 7 (1), 185–205. https://doi.org/10.1146/annurev-marine-010213-135126.

Benner, R., Biddanda, B., Black, B., McCarthy, M., 1997. Abundance, size distribution, and stable carbon and nitrogen isotopic compositions of marine organic matter isolated by tangential-flow ultrafiltration. Mar. Chem. 57 (3–4), 243–263. https://doi.org/10.1016/S0304-4203(97)00013-3.

Bourgoin, L.-H., Tremblay, L., 2010. Bacterial reworking of terrigenous and marine organic matter in estuarine water columns and sediments. Geochim. Cosmochim. Acta 74 (19), 5593–5609. https://doi.org/10.1016/j.gca.2010.06.037.

Broek, T.A.B., 2019. New Perspectives on the Composition and Cycling of Dissolved Organic Carbon and Nitrogen in the Ocean. University of California, Santa Cruz.

Broek, T.A.B., McCarthy, M.D., 2014. A new approach to δ15N compound-specific amino acid trophic position measurements: preparative high pressure liquid chromatography technique for purifying underivatized amino acids for stable isotope analysis. Limnol. Oceanogr. Methods 12 (12), 840–852. https://doi.org/10.4319/lom.2014.12.840.

Broek, T.A.B., Walker, B.D., Andreasen, D.H., McCarthy, M.D., 2013. High-precision measurement of phenylalanine δ15N values for environmental samples: a new approach coupling high-pressure liquid chromatography purification and elemental analyzer isotope ratio mass spectrometry. Rapid Commun. Mass Spectrom. 27 (21), 2327–2337. https://doi.org/10.1002/rcm.6695.

Broek, T.A.B., Walker, B.D., Guilderson, T.P., McCarthy, M.D., 2017. Coupled ultrafiltration and solid phase extraction approach for the targeted study of semi-labile high molecular weight and refractory low molecular weight dissolved organic matter. Mar. Chem. 194, 146–157. https://doi.org/10.1016/j.marchem.2017.06.007.

Broek, T.A.B., Bour, A.L., Ianiri, H.L., Guilderson, T.P., McCarthy, M.D., 2019. Amino acid enantiomers in old and young dissolved organic matter: implications for a microbial nitrogen pump. Geochim. Cosmochim. Acta 247, 207–219. https://doi.org/10.1016/j.gca.2018.12.037.

Broek, T.A.B., Walker, B.D., Guilderson, T.P., Vaughn, J.S., Mason, H.E., McCarthy, M.D., 2020. Low molecular weight dissolved organic carbon: aging, compositional changes, and selective utilization during Global Ocean circulation. Glob. Biogeochem. Cycles 34 (6). https://doi.org/10.1029/2020GB006547.

Calleja, M.Ll., Batista, F., Peacock, M., Kudela, R., McCarthy, M.D., 2013. Changes in compound specific δ15N amino acid signatures and D/L ratios in marine dissolved organic matter induced by heterotrophic bacterial reworking. Mar. Chem. 149, 32–44. https://doi.org/10.1016/j.marchem.2012.12.001.

Cava, F., Lam, H., de Pedro, M.A., Waldor, M.K., 2011. Emerging knowledge of regulatory roles of D-amino acids in bacteria. Cell. Mol. Life Sci. 68 (5), 817–831. https://doi.org/10.1007/s00018-010-0571-8.

Cowie, G.L., Hedges, J.I., 1994. Biochemical indicators of diagenetic alteration in natural organic matter mixtures. Nature 369, 304–307.

Dauwe, B., Middelburg, J.J., 1998. Amino acids and hexosamines as indicators of organic matter degradation state in North Sea sediments. Limnol. Oceanogr. 43 (5), 782–798. https://doi.org/10.4319/lo.1998.43.5.0782.

Dauwe, B., Middelburg, J.J., Herman, P.M.J., Heip, C.H.R., 1999. Linking diagenetic alteration of amino acids and bulk organic matter reactivity. Limnol. Oceanogr. 44 (7), 1809–1814. https://doi.org/10.4319/lo.1999.44.7.1809.

Davis, J., Kaiser, K., Benner, R., 2009. Amino acid and amino sugar yields and compositions as indicators of dissolved organic matter diagenesis. Org. Geochem. 40 (3), 343–352. https://doi.org/10.1016/j.orggeochem.2008.12.003.

Décima, M., Landry, M.R., Bradley, C.J., Fogel, M.L., 2017. Alanine δ15N trophic fractionation in heterotrophic protists. Limnol. Oceanogr. 62 (5), 2308–2322. https://doi.org/10.1002/lno.10567.

Dittmar, T., 2015. Reasons behind the long-term stability of dissolved organic matter. In: Biogeochemistry of Marine Dissolved Organic Matter, 2nd ed., pp. 369–385.

Gruber, D.F., Simjouw, J.-P., Seitzinger, S.P., Taghon, G.L., 2006. Dynamics and characterization of refractory dissolved organic matter produced by a pure bacterial culture in an experimental predator-prey system. Appl. Environ. Microbiol. 72 (6), 4184–4191. https://doi.org/10.1128/AEM.02882-05.

Hansell, D., Carlson, C., 1998. Deep ocean gradients in dissolved organic carbon concentrations. Nature 395, 263–266. https://doi.org/10.1038/26200.

Hébert, M., Tremblay, L., 2017. Production and persistence of bacterial and labile organic matter at the hypoxic water-sediment interface of the St. Lawrence estuary: persistence of OM in hypoxic deep waters. Limnol. Oceanogr. 62 (5), 2154–2167. https://doi.org/10.1002/lno.10556.

Jiao, N., Herndl, G.J., Hansell, D.A., Benner, R., Kattner, G., Wilhelm, S.W., Kirchman, D. L., Weinbauer, M.G., Luo, T., Chen, F., Azam, F., 2010. Microbial production of recalcitrant dissolved organic matter: long-term carbon storage in the global ocean. Nat. Rev. Microbiol. 8 (8), 593–599. https://doi.org/10.1038/nrmicro2386.

Jiao, N., Azam, F., Sanders, S. (Eds.)., 2011. Microbial carbon pump in the ocean. Science/AAAS. https://doi.org/10.1126/science.opms.sb0001.

Jørgensen, N.O.G., Stepanaukas, R., Pedersen, A.-G.U., Hansen, M., Nybroe, O., 2003. Occurrence and degradation of peptidoglycan in aquatic environments. FEMS Microbiol. Ecol. 46 (3), 269–280. https://doi.org/10.1016/S0168-6496(03)00194-6.

Kaiser, K., Benner, R., 2005. Hydrolysis-induced racemization of amino acids. Limnol. Oceanogr. Methods 3 (8), 318–325. https://doi.org/10.4319/lom.2005.3.318.

Kaiser, K., Benner, R., 2008. Major bacterial contribution to the ocean reservoir of detrital organic carbon and nitrogen. Limnol. Oceanogr. 53 (1), 99–112. https://doi.org/10.4319/lo.2008.53.1.0099.

Kaiser, K., Benner, R., 2009. Biochemical composition and size distribution of organic matter at the Pacific and Atlantic time-series stations. Mar. Chem. 113 (1–2), 63–77. https://doi.org/10.1016/j.marchem.2008.12.004.

Kawasaki, N., Benner, R., 2006. Bacterial release of dissolved organic matter during cell growth and decline: molecular origin and composition. Limnol. Oceanogr. 51 (5), 2170–2180. https://doi.org/10.4319/lo.2006.51.5.2170.

Kawasaki, N., Sohrin, R., Ogawa, H., Nagata, T., Benner, R., 2011. Bacterial carbon content and the living and detrital bacterial contributions to suspended particulate organic carbon in the North Pacific Ocean. Aquat. Microb. Ecol. 62 (2), 165–176. https://doi.org/10.3354/ame01462.

Knapp, A.N., Sigman, D.M., Kustka, A.B., Sañudo-Wilhelmy, S.A., Capone, D.G., 2012. The distinct nitrogen isotopic compositions of low and high molecular weight marine DON. Mar. Chem. 136–137, 24–33. https://doi.org/10.1016/j.marchem.2012.05.001.

Lam, H., Oh, D.-C., Cava, F., Takacs, C.N., Clardy, J., de Pedro, M.A., Waldor, M.K., 2009. D-amino acids govern stationary phase cell wall remodeling in bacteria. Science 325 (5947), 1552–1555. https://doi.org/10.1126/science.1178123.

Lechtenfeld, O.J., Kattner, G., Flerus, R., McCallister, S.L., Schmitt-Kopplin, P., Koch, B. P., 2014. Molecular transformation and degradation of refractory dissolved organic matter in the Atlantic and Southern Ocean. Geochim. Cosmochim. Acta 126, 321–337. https://doi.org/10.1016/j.gca.2013.11.009.

Lechtenfeld, O.J., Hertkorn, N., Shen, Y., Witt, M., Benner, R., 2015. Marine sequestration of carbon in bacterial metabolites. Nat. Commun. 6 (1), 6711. https://doi.org/10.1038/ncomms7711.

Lee, C., Bada, J.L., 1977. Dissolved amino acids in the equatorial Pacific, the Sargasso Sea, and Biscayne Bay. Limnol. Oceanogr. 22 (3), 502–510. https://doi.org/10.4319/lo.1977.22.3.0502.

Lee, C., Cronin, C., 1982. The vertical flux of particulate organic nitrogen in the sea: decomposition of amino acids in the Peru upwelling area and the equatorial Atlantic. J. Mar. Res. 40, 227–251.

Lehmann, M., Carstens, D., Deek, A., McCarthy, M., Schubert, C., Zopfi, J., 2020. Amino acid and amino sugar compositional changes during in vitro degradation of algal organic matter indicate rapid bacterial re-synthesis. Geochim. Cosmochim. Acta 283. https://doi.org/10.1016/j.gca.2020.05.025.

Loh, A.N., Bauer, J.E., Druffel, E.R.M., 2004. Variable ageing and storage of dissolved organic components in the open ocean. Nature 430 (7002), 877–881. https://doi.org/10.1038/nature02780.

McCarthy, M.D., Bronk, D., 2008. Analytical methods for the study of nitrogen. In: Nitrogen in the Marine Environment, 2nd. Academic Press, pp. 1219–1275.

McCarthy, M.D., Hedges, J.I., Benner, R., 1996. Major biochemical composition of dissolved high molecular weight organic matter in seawater. Mar. Chem. 55 (3), 281–297. https://doi.org/10.1016/S0304-4203(96)00041-2.

McCarthy, M.D., Pratum, T., Hedges, J.I., Benner, R., 1997. Chemical composition of dissolved organic nitrogen in the ocean. Nature 390 (6656), 150–154. https://doi.org/10.1038/36535.

McCarthy, M.D., Hedges, J.I., Benner, R., 1998. Major bacterial contribution to marine dissolved organic nitrogen. Science 281 (5374), 231–234. https://doi.org/10.1126/science.281.5374.231.

McCarthy, M.D., Benner, R., Lee, C., Fogel, M.L., 2007. Amino acid nitrogen isotopic fractionation patterns as indicators of heterotrophy in plankton, particulate, and dissolved organic matter. Geochim. Cosmochim. Acta 71 (19), 4727–4744. https://doi.org/10.1016/j.gca.2007.06.061.

McCarthy, M.D., Lehman, J., Kudela, R., 2013. Compound-specific amino acid δ15N patterns in marine algae: tracer potential for cyanobacterial vs. eukaryotic organic nitrogen sources in the ocean. Geochim. Cosmochim. Acta 103, 104–120. https://doi.org/10.1016/j.gca.2012.10.037.

Nagata, T., Meon, B., Kirchman, L., D., 2003. Microbial degradation of peptidoglycan in seawater. Limnol. Oceanogr. 48 (2), 745–754. https://doi.org/10.4319/lo.2003.48.2.0745.

Nguyen, R.T., Harvey, H.R., 1997. Protein and amino acid cycling during phytoplankton decomposition in oxic and anoxic waters. Org. Geochem. 27 (3–4), 115–128. https://doi.org/10.1016/S0146-6380(97)00076-4.

Ogawa, H., Amagai, Y., Koike, I., Kaiser, K., Benner, R., 2001. Production of refractory dissolved organic matter by bacteria. Science 292 (5518), 917–920.

Pèrez, M.T., Pausz, C., Herndl, G.J., 2003. Major shift in bacterioplankton utilization of enantiomeric amino acids between surface waters and the ocean's interior. Limnol. Oceanogr. 48 (2), 755–763. https://doi.org/10.4319/lo.2003.48.2.0755.

Peter, S., Shen, Y., Kaiser, K., Benner, R., Durisch-Kaiser, E., 2012. Bioavailability and diagenetic state of dissolved organic matter in riparian groundwater. J. Geophys. Res. Biogeosci. 117 (G4), n/a-n/a. https://doi.org/10.1029/2012JG002072.

R Core Team, 2021. *R: A Language and Environment for Statistical Computing* (4.0.5) [Computer software]. R Foundation for Statistical Computing. https://www.R-project.org/.

Radkov, A.D., Moe, L.A., 2014. Bacterial synthesis of d-amino acids. Appl. Microbiol. Biotechnol. 98 (12), 5363–5374. https://doi.org/10.1007/s00253-014-5726-3.

Schleifer, K.H., Kandler, O., 1972. Peptidoglycan types of bacterial cell walls and their taxonomic implications. Bacteriol. Rev. 36 (4), 407–477.

Shen, Y., Benner, R., Murray, A.E., Gimpel, C., Greg Mitchell, B., Weiss, E.L., Reiss, C., 2017. Bioavailable dissolved organic matter and biological hot spots during austral winter in Antarctic waters. J. Geophys. Res. Oceans 122 (1), 508–520. https://doi.org/10.1002/2016JC012301.

Shen, Y., Guilderson, T.P., Sherwood, O.A., Castro, C.G., Chavez, F.P., McCarthy, M.D., 2021. Amino acid δ13C and δ15N patterns from sediment trap time series and deep-sea corals: implications for biogeochemical and ecological reconstructions in paleoarchives. Geochim. Cosmochim. Acta S0016703720307250. https://doi.org/10.1016/j.gca.2020.12.012.

Silfer, J.A., Engel, M.H., Macko, S.A., Jumeau, E.J., 1991. Stable carbon isotope analysis of amino acid enantiomers by conventional isotope ratio mass spectrometry and combined gas chromatography/isotope ratio mass spectrometry. Anal. Chem. 63 (4), 370–374. https://doi.org/10.1021/ac00004a014.

Takano, Y., Kashiyama, Y., Ogawa, N.O., Chikaraishi, Y., Ohkouchi, N., 2010. Isolation and desalting with cation-exchange chromatography for compound-specific nitrogen isotope analysis of amino acids: application to biogeochemical samples. Rapid Commun. Mass Spectrom. 24 (16), 2317–2323. https://doi.org/10.1002/rcm.4651.

Tremblay, L., Benner, R., 2006. Microbial contributions to N-immobilization and organic matter preservation in decaying plant detritus. Geochim. Cosmochim. Acta 70 (1), 133–146. https://doi.org/10.1016/j.gca.2005.08.024.

Tremblay, L., Benner, R., 2009. Organic matter diagenesis and bacterial contributions to detrital carbon and nitrogen in the Amazon River system. Limnol. Oceanogr. 54 (3), 681–691. https://doi.org/10.4319/lo.2009.54.3.0681.

Ueda, K., Morgan, S.L., Fox, A., Gilbart, J., Sonesson, A., Larsson, L., Odham, G., 1989. D-alanine as a chemical marker for the determination of streptococcal cell wall levels in mammalian tissues by gas chromatography/negative ion chemical ionization mass spectrometry. Anal. Chem. 61 (3), 265–270. https://doi.org/10.1021/ac00178a015.

Walker, B.D., Beaupré, S.R., Guilderson, T.P., Druffel, E.R.M., McCarthy, M.D., 2011. Large-volume ultrafiltration for the study of radiocarbon signatures and size vs. age relationships in marine dissolved organic matter. Geochim. Cosmochim. Acta 75 (18), 5187–5202. https://doi.org/10.1016/j.gca.2011.06.015.

Walker, B.D., Guilderson, T.P., Okimura, K.M., Peacock, M.B., McCarthy, M.D., 2014. Radiocarbon signatures and size–age–composition relationships of major organic matter pools within a unique California upwelling system. Geochim. Cosmochim. Acta 126, 1–17. https://doi.org/10.1016/j.gca.2013.10.039.

Walker, B.D., Primeau, F., Beaupré, S.R., Guilderson, T.P., Druffel, E.R.M., McCarthy, M. D., 2016. Linked changes in marine dissolved organic carbon molecular size and radiocarbon age. Geophys. Res. Lett. 43 (19), 10,385–10,393. https://doi.org/10.1002/2016GL070359.

Wang, R., Zhang, Z., Sun, J., Jiao, N., 2020. Differences in bioavailability of canonical and non-canonical D-amino acids for marine microbes. Sci. Total Environ. 733, 139216 https://doi.org/10.1016/j.scitotenv.2020.139216.

Yamaguchi, Y.T., McCarthy, M.D., 2018. Sources and transformation of dissolved and particulate organic nitrogen in the North Pacific subtropical gyre indicated by compound-specific δ15N analysis of amino acids. Geochim. Cosmochim. Acta 220, 329–347. https://doi.org/10.1016/j.gca.2017.07.036.

Yamashita, Y., Tanoue, E., 2008. Production of bio-refractory fluorescent dissolved organic matter in the ocean interior. Nat. Geosci. 1 (9), 579–582. https://doi.org/10.1038/ngeo279.

Zhang, Z., Zheng, Q., Jiao, N., 2016. Microbial D-amino acids and marine carbon storage. Sci. China Earth Sci. 59 (1), 17–24. https://doi.org/10.1007/s11430-015-5155-x.